Review

Spectroscopy and bonding in ternary metal hydride complexes—Potential hydrogen storage media

Stewart F. Parker *

ISIS Facility, STFC Rutherford Appleton Laboratory, Chilton, Didcot, Oxon OX11 0QX, UK

Contents

ARTICLE INFO

ABSTRACT

Of the challenges that are still to be met to enable the widespread use of H_2 as a fuel for automotive applications, a safe, reliable and cheap method for its storage and transportation is paramount. This need has prompted a massive effort in the synthesis and characterisation of novel hydrides and a better understanding of existing materials. In this review the vibrational spectroscopy and the bonding of a wide range of ternary metal hydride complexes are discussed. The spectroscopic techniques used include transmission and photoacoustic infrared spectroscopy, Raman spectroscopy with excitation wavelengths ranging from 1064 to 515 nm, inelastic neutron scattering spectroscopy and nuclear resonant inelastic X-ray scattering spectroscopy. The systems studied are: the octahedral transition metal hydrides, other geometry's of transition metal hydrides, alkali metal, alkaline earth and aluminium compounds with the borohydride ion, the alkali metal and alkaline earth alanates and the alkali metal gallates. In all cases, while the central atom is the most important determinant of the properties, it has become increasingly clear that the counter-ion is much more than just a spectator; it often plays a key role in determining the stability of the material. As such, varying the counter-ion provides an important mechanism for optimising the desired properties and these are reflected in the spectra. In addition to its use in characterising materials, vibrational spectroscopy is used to investigate reactions and processes. The advantages of vibrational spectroscopy lie in its flexibility: it is not restricted to crystalline systems, amorphous or nanocrystalline materials are readily observable, it is amenable to *in situ* studies, it is democratic; infrared and Raman spectroscopy are not element specific and uniquely among probes they are able to follow a reaction across a change of state. Vibrational spectroscopy and *ab initio* calculations are a synergistic pairing. Comparison of computed and experimental spectra provides a stringent test of the calculation, while the calculation provides unambiguous assignments of the spectra. Generation of the inelastic neutron scattering spectrum provides the most reliable test since only the amplitude of motion of the atoms in each mode is required.

© 2009 Elsevier B.V. All rights reserved.

* Fax: +44 1235 445120.
  E-mail address: stewart.parker@stfc.ac.uk.

1. Introduction

Of the challenges that are still to be met to enable the widespread use of H_2 as a fuel for automotive applications [1], a safe, reliable and cheap method for its transportation is paramount. The US Department of Energy (DOE) has set targets [2] for a number of parameters that must be met for a commercially viable storage material. These include: the wt% hydrogen, the reversibility of the system, the minimum temperature and H_2 pressure needed for absorption/desorption, the H_2 charging and discharging rate, the number of times the system can be cycled from one quarter full to completely full and the purity of the released H_2. All of these targets are important but the first that must be met is a material that contains sufficient hydrogen. For 2010 the target is 4.5 wt% hydrogen for the *complete* system, including tank, valves, regulators, piping, mounting brackets, insulation and any added cooling capacity. Thus the storage material needs to contain substantially more than 4.5 wt% hydrogen. For 2015 the target is 5.5 wt% hydrogen and the ultimate aim is 7.5 wt% hydrogen (in each case the other targets reversibility, *etc.* . . . . also become more stringent). The pressing need for new compounds that meet these criteria has initiated research worldwide in hydrogen storage materials.

A variety of methods have been proposed [3], which can be broadly divided into three categories: (i) storage as gaseous H_2 (ii) storage as liquid H_2 and (iii) storage in solid form. The last category can be divided into physisorption or adsorption in or on a porous material, where the interactions are largely Van der Waals forces, and absorption or chemisorption of H_2 leading to the reversible formation of a hydride, where there is chemical bonding between the hydrogen and other atoms.

Gaseous H_2 can be compressed to 800 bar [3,4] (a standard laboratory H_2 cylinder has a maximum pressure of 200 bar) in order to reach the gravimetric target for on-board utilization, although the containment systems developed to date are expensive. In addition, the very high pressure utilised leads to severe safety problems which are compounded by the safety problems of gaseous H_2 itself. Liquid H_2 requires cryogenic containment, with its concomitant weight penalty. A wide range of adsorbents are being investigated, these include carbon nanotubes and derivatives [5], clathrates [6] and metal organic framework (MOF) materials [7,8]. Most of these do not meet the DOE target, because a large amount of 'chemical scaffolding' is required in order to trap and retain the H_2 which leads to a low gravimetric capacity. Low temperature (77 K) and elevated pressure are also often needed to achieve even modest adsorption capacities.

Hydrogen-in-metal systems (where the hydrogen atom occupies an interstitial site in the metal lattice and is not bonded to a particular atom) [9] such as PdH [10] or $LaNi_5H_6$ [11] are attractive because they are stable and readily reversible, unfortunately, they do not meet the DOE target because of the mass of metal. In a ternary metal hydride, $A_x[TH_y]$ or $A_x(MH_y)$ (A = alkali or alkaline earth metal, T = transition metal, M = B, Al or Ga) the use of a lighter Group I or II element increases the gravimetric density, this can be further increased by the use of B or Al as the atom to which hydrogen is bonded. Most metallic hydrides absorb hydrogen up to a hydrogen-to-metal ratio of 2. Compounds with a hydrogen to metal ratio of >2 (up to 4.5 in $Ba[ReH_9]$ is known) are all ionic or covalent complex hydrides, as opposed to hydrogen-in-metal systems. This has prompted an intense effort in the synthesis and characterisation of novel ternary hydrides [12–15]. The hydrides offer ways of tailoring the properties of the material by changing either (or both) the central metal atom or the counter-ion. The current view [16] is that the best candidates for hydrogen storage materials are the borohydrides and alanates. The most important reasons are illustrated in Fig. 1 that compares the volumetric and gravimetric H_2 density for a variety of systems and methods. The highest

volumetric hydrogen density known today is 150 kg m^{-3} found in $Mg_2[FeH_6]$ and $Al(BH_4)_3$, which is more than double that of liquid hydrogen, while $Li(BH_4)$ has the highest gravimetric hydrogen density of 18 wt%. Other benefits of the use of metal hydride complexes include the absence of elements, such as halides, that can lead to undesirable side reactions that both reduce the amount of H_2 available to use and may be corrosive or toxic; the formation of ammonia from amides or imides is a case in point (although borohydrides can give diborane as a highly undesirable by-product).

Another reason for interest in these materials is the possibility of new chemistry with the compounds as exemplified by the large number of derivatives of the $[ReH_9]^{2-}$ ion [17] and the extensive use of $Li(AlH_4)$ and $Na(BH_4)$ as reducing agents in organic chemistry [18].

The syntheses and structures of the compounds have been extensively reviewed [12–15]. The focus of this review is the vibrational spectroscopy of the materials. In this review we will first consider the vibrational spectroscopy of the $A_2[TH_6]$ complexes, since these form the most extensively studied hydrides and show the effect of varying both the alkali or alkaline earth metal, A, and the transition metal, T. Transition metal complexes of other stoichiometries will then be considered. The spectroscopy of the ternary borohydrides, alanates and gallates is then discussed.

2. Survey of ternary metal hydride complexes

Fig. 2 shows the transition elements for which ternary metal hydrides are known (coloured red or blue). For some elements, several complexes are known, thus ruthenium forms octahedral complexes $A_2[RuH_6]$ where A = Ca, Sr, Ba, Eu, Yb as well as quaternary complexes $CaEu[RuH_6]$ [19–21]. Palladium forms complexes with different formal oxidation states and structures: $A_2[PdH_2]$ (A = Li, Na) with linear $[PdH_2]^{2-}$ ions [22,23], $BaNa[PdH_3]$ with trigonal planar $[PdH_3]^{3-}$ ions [24] and $Ba_2[PdH_4]$ with tetrahedral $[PdH_4]^{4-}$ ions [25], which are all contain formally zero valent Pd, in addition there are $A_2[PdH_4]$ complexes [26,27] (A = Na, K, Rb) with square planar $[PdH_4]^{2-}$ ions, which contain formally divalent Pd. Those elements for which at least one complex has been studied by vibrational spectroscopy are shown in red.

What is striking about Fig. 2 is the apparent dividing line at the (Mn, Tc, Re) triad. Transition elements to the left do not form complexes, instead hydrogen-in-metal systems are found, while elements to the right form an extensive array of complexes of different stoichiometries, geometries and oxidation states. This division may be artificial; recent work [28] has produced evidence that a $Mg_3[CrH_6]$ complex is formed at 8 GPa, although the hydrides were not located. Many of the elements to the right of the (Mn, Tc, Re) triad form hydrogen-in-metal compounds depending on the hydrogen to metal ratio. Thus Mg_2Ni initially reacts with H_2 to give $Mg_2NiH_{0.3}$ while it forms $Mg_2[NiH_4]$ with excess H_2 [29]. Similarly, YMn_2 forms a series of solid solutions [30] YMn_2H_x ($0.1 \leq x \leq 0.43$) at a few bar H_2 pressure at room temperature but forms $(YMn)[MnH_6]$ at 0.2 GPa and 473 K [31]. Together, these observations suggest that compound formation to the left of (Mn, Tc, Re) may be possible but that it requires much more forcing conditions than for the elements to the right of, and including (Mn, Tc, Re).

3. Vibrational spectroscopy and *ab initio* methods

A variety of vibrational spectroscopies have been used to study the compounds. These include infrared, Raman, inelastic neutron scattering (INS) and nuclear resonant inelastic X-ray scattering (NRIXS) spectroscopies. Infrared spectra are usually obtained from mulls or KBr discs, although special precautions to exclude air
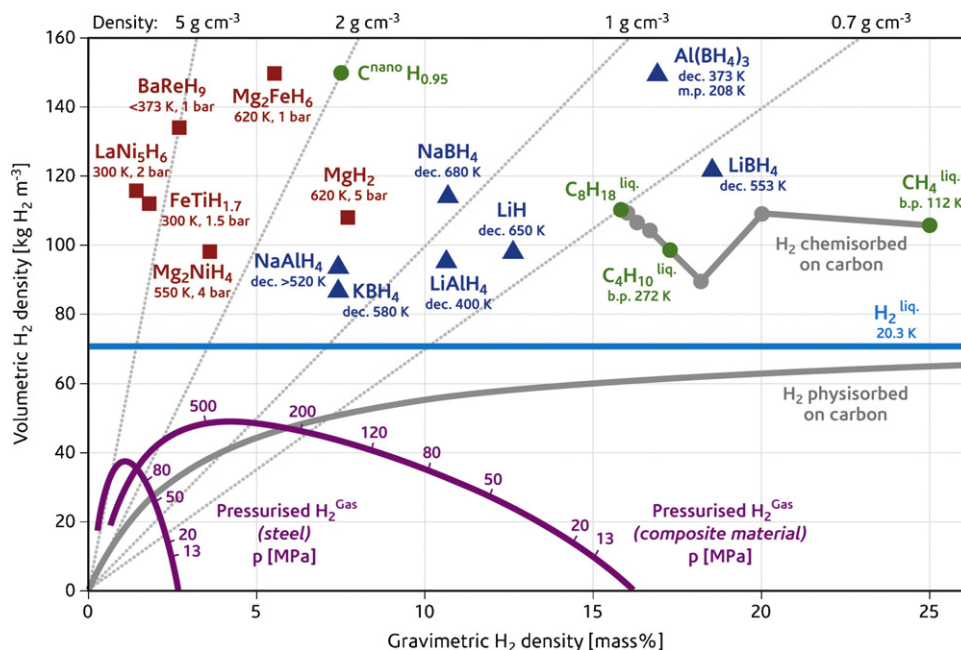
Fig. 1. Volumetric and gravimetric hydrogen density of some selected hydrides. Pressurized gas storage is shown for steel (tensile strength = 460 MPa, density 6500 kg m⁻³) and a hypothetical composite material (tensile strength = 1500 MPa, density 3000 kg m⁻³). Reproduced from Ref. [16] with permission of Springer-Verlag.

and moisture are often needed [32]. A recent development was the use of photoacoustic infrared spectroscopy [33] which has the advantage of using the pure compound, so allowing weak bands to be observed. Raman spectra have been recorded with conventional dispersive instruments using green (514.5 nm) [34] or red (785 nm) excitation [35] as well as by Fourier transform Raman spectroscopy with 1064 nm excitation [32,34] to reduce fluorescence backgrounds. INS spectroscopy [36] has several advantages that make it ideal for the study of ternary metal hydrides. The observed intensity of an INS spectral band, S, is a function of both the energy, ω, and the momentum, Q, exchanged during the scattering process and is given by [36]:

$$S(Q, n\omega_i) \propto \frac{(QU_i)^{2n}}{n!} \exp(-(QU_{Tot})^2)\sigma \qquad (1)$$

where ω_i is the ith mode at wavenumber ω, $n = 1, 2, 3, 4, \ldots, \infty$ ($n = 1$ for a fundamental, 2 for a first overtone or binary combination, 3 for a second overtone or ternary combination, *etc.* . . . in practice the approximation that $n = 10 = \infty$ is usually made since higher order transitions contribute little intensity in the 0–4000 cm⁻¹ region for experimentally accessible Q values), U_i is the root mean square displacement of the atoms in the mode, U_{Tot} is the total root mean square displacement of all the atoms in all the modes, both internal and external, σ is the inelastic scattering cross section of the atom. The cross section is both element and isotope dependent [37]; for ¹H it is 82.02 barn (1 barn = 1 × 10⁻²⁸ m²), for ²H it is 7.64 barn and for most other elements it is 5–12 barn. Since hydrogen is both the lightest element (hence has the largest amplitude of vibration) and has the largest cross section, motions that involve hydrogen will dominate the spectrum. Further, Eq. (1) is purely dynamic, thus the

symmetry requirements that give rise to selection rules for infrared and Raman spectroscopies are absent and all modes are allowed. In INS spectroscopy, overtones and combination bands are allowed transitions in the harmonic approximation.

Infrared and Raman bands are observed at the Brillouin zone centre and since acoustic modes have zero wavenumber at the Brillouin zone centre they are unobservable by these methods. In contrast, INS spectroscopy is sensitive to modes at all wavevectors across the Brillouin zone and acoustic modes may be observed. The INS spectrum is the amplitude-of-motion and cross section weighted vibrational density of states. To a first approximation, this is given by the projection of the dispersion curves onto the energy axis. This has the result that undispersed modes, of which internal vibrations are typical, give sharp lines, whereas dispersed features give broader, structured features, potentially giving insight into the long range interactions present in the material. Some of the INS spectra of ternary metal hydrides are available at http://www.isis.rl.ac.uk/insdatabase.

NRIXS combines nuclear excitation and vibrational motion [39]. When a Mössbauer nucleus is excited by a suitable energy photon, it can also excite a vibrational mode. The requirement for a tunable X-ray source and high resolution (a mode at 1000 cm⁻¹ coupled to the 14.4 keV excitation of ⁵⁷Fe results in a shift of only 0.0017% in energy) means that such experiments are only feasible at a synchrotron. The measurement provides isotope selective vibrational spectra; only modes with movement of the resonant nucleus couple to the excitation. In practice, this means that most measurements to date have used ⁵⁷Fe as the Mössbauer isotope.

One of the advantages of vibrational spectroscopy is that it offers insights into the bonding present in materials. While the

Sc	Ti	V	Cr	Mn	Fe	Ni	Co	Cu	Zn
Y	Zr	Nb	Mo	Tc	Ru	Pd	Rh	Ag	Cd
La	Hf	Ta	W	Re	Os	Pt	Ir	Au	Hg

Fig. 2. Part of the periodic table showing the transition elements: those that form ternary metal hydrides are coloured red or blue, those where at least one compound has been studied by vibrational spectroscopy are shown in red. (For interpretation of the references to color in this figure legend, the reader is referred to the web version of the article.)

Table 1
Observed frequencies, assignments and properties for octahedral $A_x[MH_6]$ compounds.

Complex	ν_1 M–H stretch (a_{1g}, R) [a]	ν_2 M–H stretch (e_g, R)	ν_3 M–H stretch (t_{1u}, IR)	ν_4 M–H bend (t_{1u}, IR)	ν_5 M–H bend (t_{2g}, R)	ν_6 M–H bend (t_{2u}, ia)	ν_{lib} (t_{1g}, ia)	ν_{trans} (t_{2g}, R)	ν_{trans} (t_{1u}, IR)	$\nu_{acoustic}$ (t_{1u}, ia)	M–H distance (Å)	Reference
$Mg_2[FeH_6]$	1873	1873	1746	899	1019/1057	836	460 broad	223	157	103	1.556	[46]
$[MgBr(THF)_2]_4[FeH_6]$ [b]			1569/1523	787 [c]				357 [c]	212 [c]		1.609[c]	[61,62]
$[Mg(O^tBu)(THF)_2]_4[FeH_6]$ [b]			1413									[61]
$Mg_2[RuH_6]$			1783								1.67	[21]
$[MgBr(THF)_2]_4[RuH_6]$[b]			1562								1.85	[61]
$Ca_2[RuH_6]$	1833	1754	1564	896	867	867	537	201	175		1.709	[33,47,49]
$Sr_2[RuH_6]$	1782	1731	1487	890	856	856	561				1.69	[33,47,49]
$Ba_2[RuH_6]$			1438								1.72	[21]
$Yb_2[RuH_6]$			1550	886								[48]
$Eu_2[RuH_6]$	1785	1713	1462	874	840	{851}[d]	{522}				1.68	[33,47,49]
$Mg_2[OsH_6]$			1849	864							1.728	[21]
$Ca_2[OsH_6]$			1637									[21]
$Sr_2[OsH_6]$			1575									[21]
$Ba_2[OsH_6]$			1505									[21]
$Na_2[PtH_6]$[e]	(2083)		(1785)	(901)	(861)	{(823)}					1.615	[32]
$K_2[PtH_6]$	2050		1748	881	840	{808}					1.640	[32]
$Rb_2[PtH_6]$	2044	2074	1743	877	828	828	366	90	108	40	1.629	[38]

[a] The irreducible representation to which the mode belongs (in point group O_h) and the activity of the mode are shown in brackets. R: Raman allowed, IR: infrared allowed, ia: inactive in both the infrared and Raman spectrum.
Note: that *all* modes are allowed in the INS spectrum.
[b] Complex does not crystallise in space group $Fm\bar{3}m \equiv O_h^5$, hence symmetry labels are not applicable.
[c] Average Fe–H distance, see Ref. [59].
[d] Values in curly brackets are estimated from combination bands; see text.
[e] Calculated from the frequencies of the deuteride assuming an isotopic shift of 1.397 (the average of that for the potassium and rubidium salts).

compounds have also been the subject of many theoretical investigations, *e.g.* [38,40–45], the most stringent test of a calculation is to compare the predicted and observed vibrational spectrum. Indeed, this is the best method to demonstrate that the calculation has converged to a genuine energy minimum rather than to a saddle point on the potential energy surface. This approach is synergistic: it provides unambiguous assignments of the spectra and validates the *ab initio* calculation, giving confidence in the conclusions drawn from both.

Any *ab initio* calculation that provides vibrational frequencies will also give the atomic displacements of the atoms in each mode. This enables the modes to be visualised and also provides the U_i needed to compute the INS spectrum *via* Eq. (1). Thus it is straightforward to generate a calculated INS spectrum from *ab initio* results. Some programs are also capable of providing calculated infrared intensities, however, the routine calculation of Raman intensities is still awaited.

4. Ternary transition metal hydrides

4.1. Octahedral transition metal $A_2[TH_6]$ complexes

The octahedral $A_2[TH_6]$ complexes are the systems that have been most extensively studied by vibrational spectroscopy, as shown in Table 1. All of the compounds adopt the face centred cubic $K_2[PtCl_6]$ structure (space group $Fm\bar{3}m$, number 225), with the transition metal on the octahedral site (4*a*) and the alkali or alkaline earth metal counter-ions on the tetrahedral sites (8*c*). There are four formula units in the conventional unit cell, but only one in the primitive Bravais cell, which simplifies computational studies since only the primitive cell needs to be considered. Fig. 3 (top) shows the structure of the conventional unit cell. The high symmetry results in many of the modes being degenerate and few being infrared or Raman allowed as shown in the first row of Table 1. Note that *all* modes are allowed in the INS spectrum.

Fig. 4 shows the vibrational spectra of $Ca_2[RuH_6]$ [33] which highlights the effect of the symmetry. The Raman spectrum (Fig. 4a) and the conventional transmission (KBr pellet) infrared spectrum (Fig. 4b) both contain only a few bands. The INS spectrum (Fig. 4d) shows more features including the infrared and Raman forbidden librational mode at 537 cm^{-1}. The third bending mode, ν_6, that is also infrared and Raman forbidden, is not immediately apparent in the INS spectrum. Since it involves proton motion, it must appear in the INS spectrum. The 858 cm^{-1} band, ν_5, is almost exactly twice as intense as the 889 cm^{-1} band, ν_4, thus, the third internal mode of t_{2u} symmetry (ν_6) must be accidentally degenerate with the t_{2g} mode (ν_5) at 858 cm^{-1}. (The same situation is also found for $Rb_2[PtH_6]$ [38].) The assignment is confirmed by a periodic DFT calculation that indeed shows ν_5 and ν_6 to be accidentally degenerate (Fig. 4e).

For the octahedral $[TX_6]^{n-}$ (X = halogen, O) complexes, the usual order of the modes is $\nu_1 > \nu_2 > \nu_3$ and $\nu_4 > \nu_5 > \nu_6$ [50]. For the stretching modes, this is not always the case and for some complexes the order is: $\nu_2 > \nu_1 > \nu_3$. The difference between the hexahydrido and the hexahalo and hexaoxo complexes must lie in the mass difference between hydrogen and the other elements. For the hydride ligands there is at least a factor of 50 difference between the mass of the hydride and the central metal atom; for no other ligand is the ratio so large. This effectively decouples the M–H vibrations from each other, and in the limit of no coupling, all three stretching modes are coincident. The form of the a_{1g} and e_g (ν_1 and ν_2) modes is similar in that the modes do not involve motion of the central metal atom and adjacent M–H bonds behave as independent oscillators, in contrast, the t_{1u} mode (ν_3) involves movement by the central metal atom providing an efficient means of coupling between opposing oscillators. Thus the order $\nu_1 \approx \nu_2 > \nu_3$ would be expected and is found. For the bending
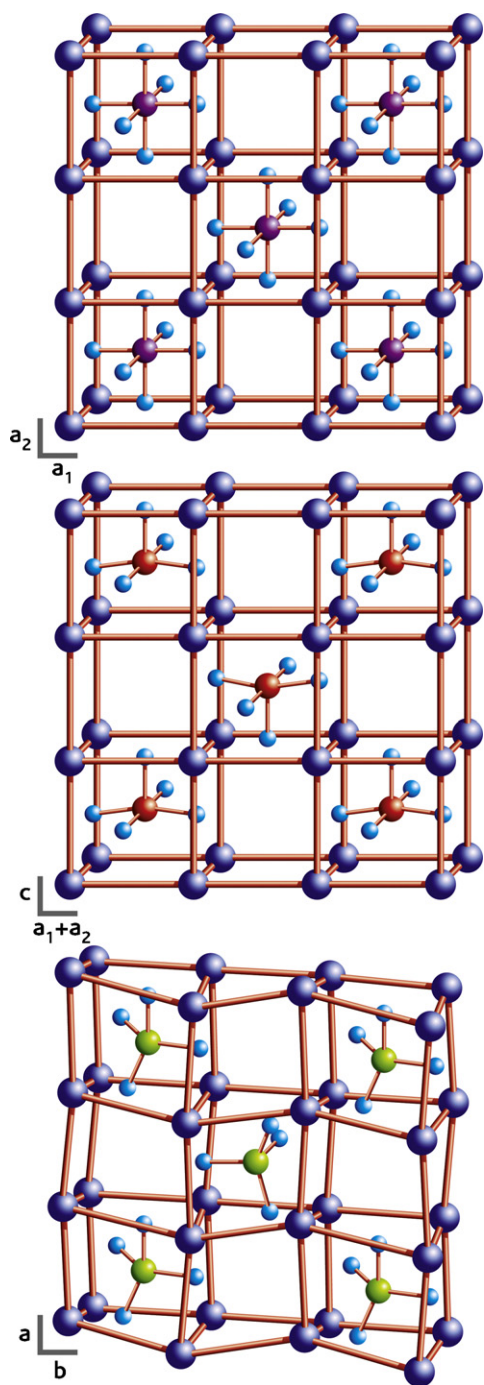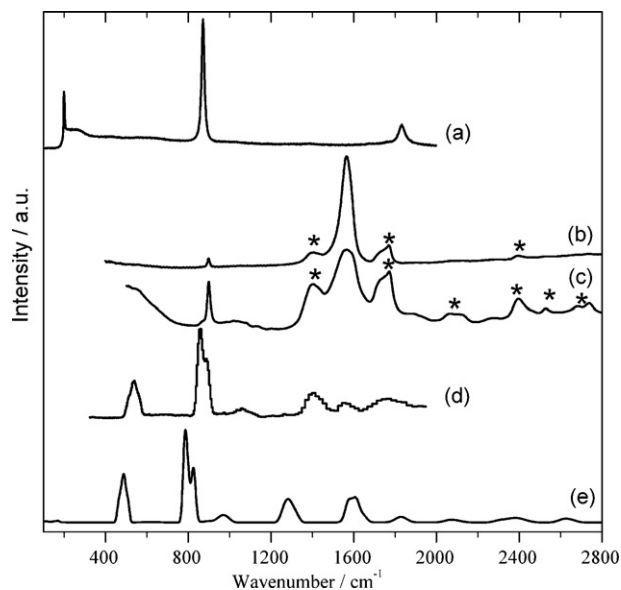
Fig. 3. Structures of compounds: (top) face centred cubic $A_2[TH_6]$, (middle) $Mg_2[CoH_5]$ and (bottom) $Mg_2[NiH_4]$.

Fig. 4. Vibrational spectra of $Ca_2[RuH_6]$: (a) Raman, (b) transmission infrared (KBr pellet), (c) photoacoustic infrared, (d) INS and (e) INS spectrum generated from a periodic DFT calculation. The asterisks in (b) and (c) indicate combination bands that are visible because of Fermi resonance between the t_{1u} infrared active fundamental and a binary or ternary combination mode involving the bending modes. Reproduced from Ref. [33] with permission of the American Chemical Society.

modes, the hydrides follow the same order (except for $Mg_2[FeH_6]$, see later) as for the $[MX_6]^{n-}$ (X = halogen, O) complexes. I note that the empirical relation $\nu_6 = \nu_5/\sqrt{2}$ [51] is not followed by the hydrides (and not always by the halides [52]), generally $\nu_5 \approx \nu_6$.

One of the features of Table 1 is the scarcity of entries. Only those for which INS spectra [33,38,46] have been recorded have complete, or nearly so, data. However, the infrared spectra of the complexes [32,33,46,53] often show more bands (indicated by asterisks in Fig. 4b) in the region of the antisymmetric M–H stretch than would be predicted by group theory. While there are a number of possible reasons for the splitting: e.g. LOTO splitting, reduction of symmetry, several authors [33,38,46] have shown that the 'extra' bands are observable because of Fermi resonance [54] between the t_{1u}

infrared active fundamental and a binary or ternary combination mode involving the bending modes. For Fermi resonance to occur the direct product of the symmetries of the modes contributing to the combination must include a T_{1u} contribution. (This is why it must be a combination since $g \otimes g \to g$ and $u \otimes u \to g$ but $g \otimes u \to u$.) Of the six possible binary combinations of the lower energy modes that occur in the region of the antisymmetric stretch: $(\nu_4 + \nu_5)$, $(\nu_4 + \nu_6)$, $(\nu_5 + \nu_6)$, $(\nu_{lib} + \nu_4)$, $(\nu_{lib} + \nu_5)$, $(\nu_{lib} + \nu_6)$, only $(\nu_4 + \nu_5)$, $(\nu_5 + \nu_6)$, $(\nu_6 + \nu_{lib})$ have T_{1u} components. Thus a maximum of three additional modes would be predicted. For the $A_2[RuH_6]$ (A = Ca, Sr, Eu) salts all three modes are observed [33] and for $A_2[PtH_6]$ (A = Na, K, Rb) two modes are observed [32]. This allows estimates of the forbidden ν_6 and ν_{lib} modes to be made for the Ru salts and of ν_6 for the Pt salts and these are shown in curly brackets in Table 1. This analysis ignores the effects of anharmonicity, an indication of its magnitude can be obtained by comparison of the observed and predicted wavenumbers of the bands for the systems where all the transition energies are known from the INS spectra. Table 2 shows the comparison. It can be seen that the difference between observed and calculated frequencies is generally small, indicating that anharmonicity is not large in these systems so the calculated values are reliable to a few percent. This is supported by the shifts on deuteration that are close to the $1/\sqrt{2}$ expected for a harmonic system. The mode that shows the largest anharmonicity is the librational mode and this has consequences for ab initio calculations that will be discussed in Section 4.2.
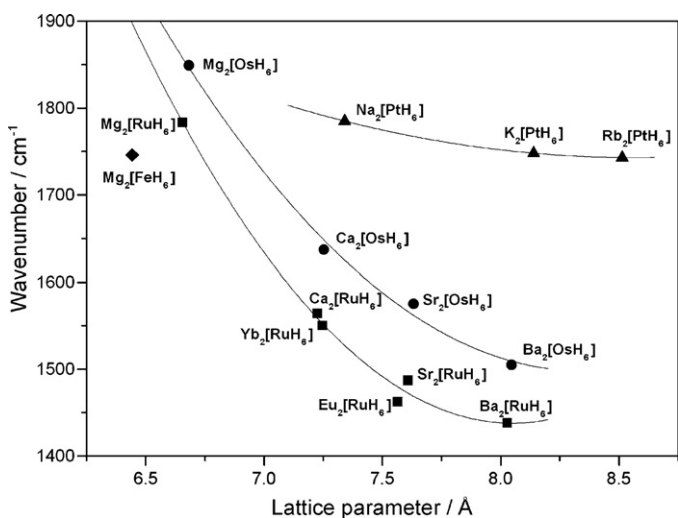
Better estimates of the infrared and Raman forbidden modes and of the anharmonicity can be obtained if more combinations are observed. Recent work [33] obtained infrared spectra by photoacoustic infrared spectroscopy, in addition to the KBr pellet technique, and the results are remarkable. Fig. 4b and c shows the infrared spectra of $Ca_2[RuH_6]$ by the two different methods. It can be seen that there are many more modes visible in the photoacoustic infrared spectrum. This presumably results from the use of the pure powder, so resulting in a much increased pathlength. If this proves to be generally the case for non-conducting ternary metal hydrides, this will provide a very useful technique for gaining considerable additional information with little additional effort.

Table 2
Comparison of observed and calculated overtones and combinations of $A_2[MH_6]$ complexes.

Mode (cm^{-1})	Mg$_2$[FeH$_6$] [46]	Ca$_2$[RuH$_6$] [33]	Sr$_2$[RuH$_6$] [33]	Rb$_2$[PtH$_6$] [38]
$(\nu_4 + \nu_5)$				
Obs.	1912	1769	1737	1708
Calc.	1918	1747	1746	1705
(Obs. – Calc.)	−6	+22	−9	+3
$(\nu_5 + \nu_6)$				
Obs.	1843	1728	1700	1640
Calc.	1855	1734	1712	1656
(Obs. – Calc.)	−12	-6	−12	−16
$(\nu_6 + \nu_{lib})$				
Obs.		1395	1371	
Calc.		1386	1417	
(Obs. – Calc.)		+9	−46	
$(2 \times \nu_{lib})$				
Obs.		1022	1075	726
Calc.		1056	1122	732
(Obs. – Calc.)		−34	−47	−6
ν_6 obs.	836	858	856	828
ν_6 calc.	824	870	844	812
ν_{lib} obs.	460	528	561	366
ν_{lib} calc.		525	540	363

A number of trends are immediately apparent from Table 1. For a given counter-ion, the wavenumbers of the stretching modes increase as the atomic number of the transition metal increases: *e.g.* for A = Mg, the antisymmetric stretching mode is at 1746, 1783 and 1849 cm^{-1} for T = Fe, Ru and Os respectively. This is not the case for the bending modes and, except for one mode of Mg$_2$[FeH$_6$], all of the modes fall in the range 830–900 cm^{-1}. For an individual metal, there is a marked dependence on the counter-ion; the stretching frequencies fall as the atomic number increases, although this is much more marked for Fe, Ru and Os than for Pt. For a given transition metal, there is a rough correlation with the M–H distance, although this is not true when different transition metals are compared.

As shown by Kritikos and Noréus [21], there is a reasonable correlation between the antisymmetric stretching mode's wavenumber and the lattice parameter (see Fig. 5). These authors attributed this to the size of the counter-ion and not its electropositivity since the values for Eu$_2$[RuH$_6$] and Yb$_2$[RuH$_6$] fell on the same curve as the alkaline earth salts of [RuH$_6$]$^{4-}$. They suggested that this was evidence for the hydride ligand having some electron-accepting properties due to the large polarizability of the metal–hydrogen bond which enables hydrogen to distribute electron density away from the proximity of the central atom by means of its potential to adopt a large radius [21]. This idea finds support in a periodic density functional theory (DFT) study of the A$_2$[PtH$_6$] (A = Li, Na, K, Rb, Cs) [38] complexes. From Table 3 it can be seen that the DFT results mirror the experimental trends. The Pt–H and M–H bond distances increase with increasing cation size. As may be expected, as the Pt–H distance increases, the Pt–H stretching mode's transition energy falls. The Pt–H bonding is largely covalent in the salts since the distances are close to the sum of the covalent radii (1.65 Å) and fall in the range typically found for platinum hydride complexes [55]. This is confirmed by inspection of the Mulliken charges which shows that the Pt carries a sizable negative charge and the hydrogen only a small positive charge in the salts which decreases with increasing atomic number of the alkali metal ion, *i.e.* the hydrogen is accepting negative charge as suggested by Kritikos and Noréus [21]. Note the distinction from the hypothetical gas phase ion (last column of Table 3) where there are no interactions with other ions for which the hydrogen carries a negative charge. However, the larger effect is due to the alkali metal ion whose role is to reduce the charge on the Pt and H, thus stabilising the complex. As the alkali metal becomes more electropositive it has an increasing charge. This would also explain the empirical observation that it is generally easier to make the complexes with K and Rb than Li or Na. Surprisingly, the calculations indicate that the trend is apparently not continued with Cs.

The role of the cation to stabilise the complex by reducing the positive charge on the metal and hydrogen has been observed before in Mg$_2$[NiH$_4$] [43] (which contains Ni(0)) and also in a series of Pd(0) hydrides [56]. Thus the same mechanism applies to both high, Pt(IV), and low valent hydrides. While in Ref. [38] was the first time it had been shown in a formally high valent complex, it suggests that this is the general case. Moyer et al. [57] extended the argument further by noting that a high electropositivity is equivalent to a low ionization energy. They plotted the antisymmetric stretching mode's wavenumber of the Ru and Os complexes against the second ionization energy of the alkaline earth or lanthanide, which was used as a measure of the electropositivity of the ion. They found a linear relation that was dependent on the central metal. They also found that the complexes lay on a common line

Fig. 5. Antisymmetric stretching mode transition energy of the cubic A$_2$[MH$_6$], complexes as a function of unit cell length. The solid lines are a guide to the eye. Adapted from Ref. [21] with permission of Elsevier.

Table 3

Comparison of observed and calculated properties of A_2PtH_6 (A = Li, Na, K, Rb, Cs). Experimental values in parentheses. Reproduced from Ref. [38] with permission of the American Chemical Society.

Property	Li	Na	K	Rb	Cs	Gas phase[a]
Lattice parameter (Å)	6.564 (6.5549)[b]	7.1716 (7.3410)	8.2002 (8.1399)	8.6222 (8.5369)	8.9503 (8.9681)	
Pauling ionic radius A (Å)	(0.60)	(0.95)	(1.33)	(1.48)	(1.69)	
Lattice energy (kJ mol^{-1})	2223	1966	1755	1665	1577	
Pt–H (Å)	1.639	1.641 (1.615)	1.644 (1.640)	1.646 (1.629)	1.647 (1.641)	1.678
A⋯H (Å)	2.354	2.540 (2.74)	2.927 (3.12)	3.091 (3.06)	3.219 (3.52)	
ν_1 Pt–D stretch a_{1g} (cm^{-1})	1673	1651 (1491)	1604 (1471)	1588 (1466)	1577	1387
Charge on Pt (e$^-$)[c]	−1.718	−1.777	−1.601	−1.511	−1.422	−1.860
Charge on A (e$^-$)	+0.370	+0.598	+0.698	+0.703	+0.536	
Charge on H (e$^-$)	+0.163	+0.097	+0.034	+0.018	+0.058	−0.232

[a] Average of isolated molecule calculation using the B3LYP functional and the SDD and LANL2DZ basis sets.

[b] By extrapolation of the Na, K, Rb and Cs salts.

[c] e$^-$: electrons.
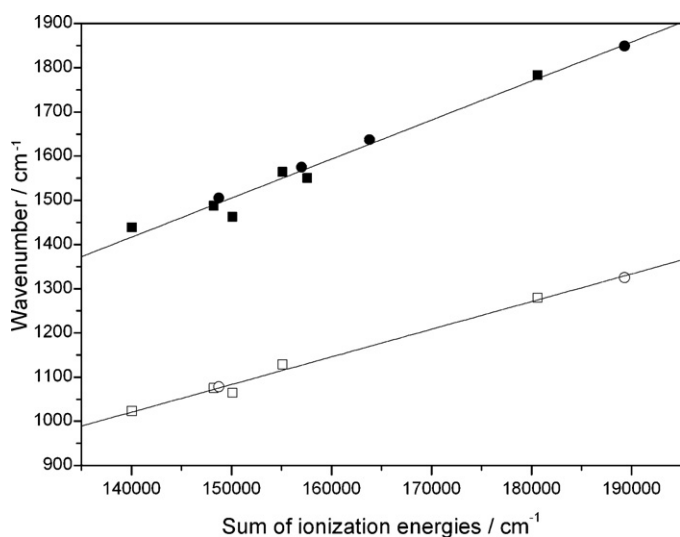
Fig. 6. Antisymmetric stretching mode transition energy of the cubic $A_2[MH_6]$ complexes *versus* the sum of the ionization energies of the alkaline earth or lanthanide and the transition metal. Squares: Ru salts; circles Os salts. Filled symbols for metal–hydrogen stretching frequencies and empty symbols for deuterium. The solid lines are linear least squares fits. Reproduced from Ref. [57] with permission of Elsevier.

if the sum of the first ionization energy of the central metal atom was added to that of the second ionization energy of the alkaline earth or lanthanide, as shown in Fig. 6.

All of the $A_2[TH_6]$ compounds studied conform to the expectations from group theory; except for $Mg_2[FeH_6]$ [46]. Fig. 7 shows the vibrational spectra of the complex. Comparison with Fig. 4 reveals several differences: the splitting of the t_{2g} (ν_5) bending mode at ~1000 cm^{-1} in both the Raman and INS spectra, $\nu_5 > \nu_4$, the asymmetry of the t_{2u} (ν_6) mode in the INS spectrum suggestive of a small splitting, the formally forbidden T_{1g} librational mode in the Raman spectrum. The complex shape of the librational mode of the $[FeH_6]^{4-}$ ion at 460 cm^{-1} in the INS spectrum is clear evidence of strong dispersion in this mode. The latter is in marked contrast to $Rb_2[PtH_6]$ where the librational mode is resolution limited in the INS spectrum [38], indicating a dispersionless mode. The presence of the splitting in the t_{2g} (ν_5) bending mode in both the room temperature Raman spectrum and the 20 K INS spectrum suggests that a phase change is not responsible for the effect. The line shape of the INS bands could be accounted for by weak dispersion in the modes, although this would not account for the splitting in the Raman spectrum. Interestingly, the vibrational spectra of $Mg_2[FeD_6]$ are completely consistent with group theory expectations. The crystal structure [58] was determined by X-ray crystallography of the protonated species, which only located the Mg and Fe ions, and neutron

powder diffraction of the deuteride which located all the atoms. One possible explanation of the observations is that the $[FeH_6]^{4-}$ octahedra are slightly tilted by a few degrees, this would leave the Mg and Fe ions in the same positions, consistent with the X-ray results, but it would change the local symmetry that the vibrational spectroscopy probes. The smaller zero point energy of the deuteride stabilises the fully symmetric structure that is expected.

All of the $A_2[TH_6]$ complexes considered so far were prepared by solid-state reactions of an alkali or alkaline earth hydride with the transition metal under a H_2 atmosphere at elevated temperature and pressure [12–15]. It is also possible to prepare soluble salts of $[TH_6]^{4-}$ (T = Fe, Ru) by the reaction of FeX_2 or $[Ru(\eta^4-1,5\text{-COD})X_2]$ (X = Cl or Br, COD = cyclooctadiene) with C_6H_5MgBr solutions under hydrogen followed by extraction with tetrahydrofuran (THF) [59–61]. This yields $[MgBr(THF)_2]_4[TH_6]$ (T = Fe, Ru) which contains a central $[TH_6]^{4-}$ ion with four of the eight triangular faces capped by $[MgX(THF)_2]^-$ ions [59], the Ru complex is presumed to be isostructural. These materials hint at the wider chemistry that may be available for ternary metal hydrides, for instance the complexes have been shown to be active hydrogenation catalysts [60,62].

As shown in Table 1, the Fe–H stretching wavenumber is dependent on the other ligands present, although the overall variation of ~300 cm^{-1} is similar to that observed for the Ru and Os complexes as the counter-ion is varied. In the crystal, the Fe ion occupies a C_2 site, so all the degeneracies are lifted and all the modes are formally allowed. However, the distortion from O_h symmetry is small (the Fe–H distances are all within 0.01 Å of each other and the adjacent H–Fe–H angles are within 1° of 90° [59]) so the O_h selection rules
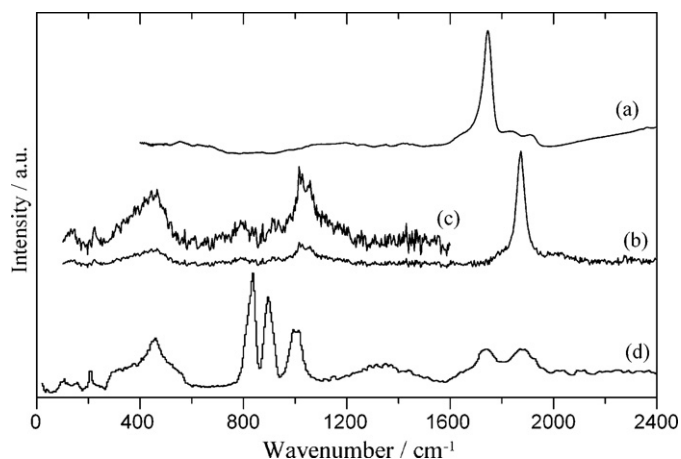
Fig. 7. Vibrational spectra of $Mg_2[FeH_6]$: (a) infrared, (b) Raman, (c) Raman ×3 ordinate expanded and (d) INS. Reproduced from Ref. [46] with permission of the American Chemical Society.

would be expected to be approximately obeyed. The only infrared mode reported [60] is derived from the t_{1u} stretch and shows some splitting. Very unusually, $[MgBr(THF)_2]_4[FeH_6]$ has also been investigated by NRIXS [62] which detected the bending mode derived from the t_{1u} bend and two translational modes, as shown in Fig. 8. These are the only modes which result in motion of the iron atom which is a pre-requisite for observation by NRIXS [39]. The bending mode is at much lower wavenumber than in $Mg_2[FeH_6]$, this differs from the alkaline earth complexes of Ru and Os where the bending modes are largely insensitive to the nature of the counter-ion.

4.2. Non-octahedral transition metal $A_x[TH_y]$ complexes

As may be seen from Table 4, which is only a small subset of the known structures [12–15], there is a wide range of structures adopted by the transition metal hydrides that are not octahedral. These less symmetrical forms have the consequence that the infrared and Raman selection rules are relaxed and many more of the modes are allowed. Note that a mode may be allowed but have little or no intensity and this is frequently the case. This is exemplified by the $[ReH_9]^{2-}$ ion: an isolated D_{3h} $[ReH_9]^{2-}$ ion has 24 vibrations, which are distributed as 16 modes: 9 Re–H stretches:

$$2A_1'(R) + 2E'(IR, R) + A_2''(IR) + E''(R)$$

and 15 H–Re–H bends

$$A_1'(R) + A_2'(ia) + 3E'(IR, R) + A_1''(ia) + 2A_2''(IR) + 2E''(R)$$
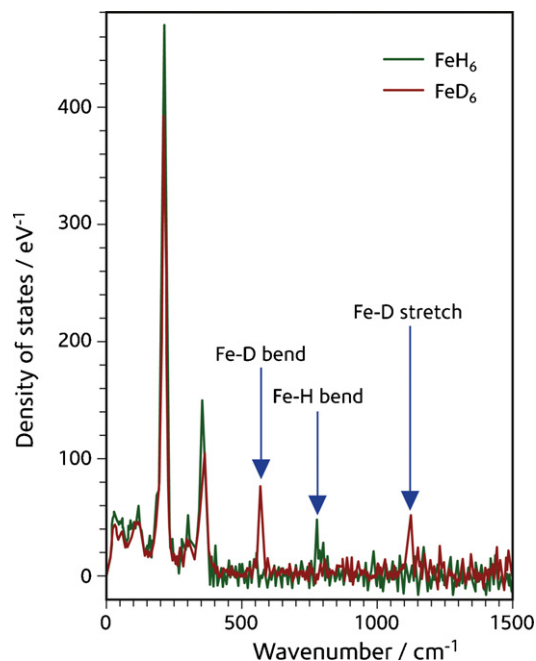
Fig. 8. NRIXS for $(MgBr(THF)_2)_4[FeH_6]$ (green trace) and $(MgBr(THF)_2)_4[FeD_6]$ (red trace). Reproduced from Hyperfine Interact. 170 (2006) 47–54 with permission of Springer.

Table 4
Observed frequencies and assignments for non-octahedral transition metal $A_x[MH_y]$compounds.

Hydride	Formal oxidation state of transition metal	Metal geometry (symmetry)	Stretching modes (symmetry)	Bending modes	Librational modes	Translational modes	Interstitial H modes	Reference
Ba[ReH₉]	+7	Face-capped trigonal prism (D_{3h})	1992, 1977, 1956, 1913, 1870, 1830	1053, 991, 920, 860, 801, 730, 680	256, 172, 136	78, 49		[67]
Na₂[ReH₉]	+7	Face-capped trigonal prism (D_{3h})	1835,	810, 745, 730, 630				[63,64]
KNa[ReH₉]	+7	Face-capped trigonal prism (D_{3h})	1950, 1854,1750,	738				[63,66]
K₂[ReH₉]	+7	Face-capped trigonal prism (D_{3h})	1975, 1956, 1924, 1880, 1840, 1710	1025, 990, 730, 670	401, 330, 229,			[64,65]
Mg₂[CoH₅]	+1	Square-based pyramid (C_{4v})	1834, 1784, 1757, 1632	1032, 869, 766	574, 532, 426,	308, 208, 140		[68]
Mg₂[NiH₄]	0	Distorted tetrahedron (C_1)	1691, 1674	791, 745, 654, 620	496, 427	299, 234, 193, 96		[70]
Li₂[PdH₂]	0	Linear ($D_{\infty h}$)	1767, 1554	783	615, 487	105		[56]
Na₂[PdH₂]	0	Linear ($D_{\infty h}$)	1663, 1448	750,720	553, 471			[56,69]
NaBa[PdH₃]	0	Trigonal planar (D_{3h})	1400, 1370	620, 470	410, 361	165, 130, 88		[56]
Ba₂[PdH₄]	0	Distorted tetrahedron (C_s)	[1332,1256,1227,1184]ᵃ	620, 590, 762, 527	515, 420			[35,56]
LaMg₂PdH₇	0	Distorted tetrahedron (C_1)	1567, 1536, 1482, 1254	725,704,438, 613, 546	527, 480, 425	176, 139, 99, 70	1158-725	[35]
K₂[PdH₄]	+2	Square planar (D_{4h})	1810, 1810, 1500,	1280, 826, 820, 820	480, 430			[34,56]
Na₂[PtH₄]	+2	Square planar (D_{4h})	2075, 2025, ~1700,	911, 845	434, 341			[34]
K₂[PtH₄]	+2	Square planar (D_{4h})	2051, 2001	839				[34]
K₃PtH₅		Square planar (D_{2h})	2100, 2039	810				[34]
Rb₂[PtH₄]	+2	Square planar (D_{4h})	2046,1990, ~1700,	859, 839	417, 291			[34]
Rb₃ZnH₅	+2	Squashed tetrahedron (D_{2d})	1530, 1470, 1449, 1386	690, 658, 627,600	318	103, 58	745, 702	[70,71]

ᵃ Calculated by periodic DFT, see text and [35].
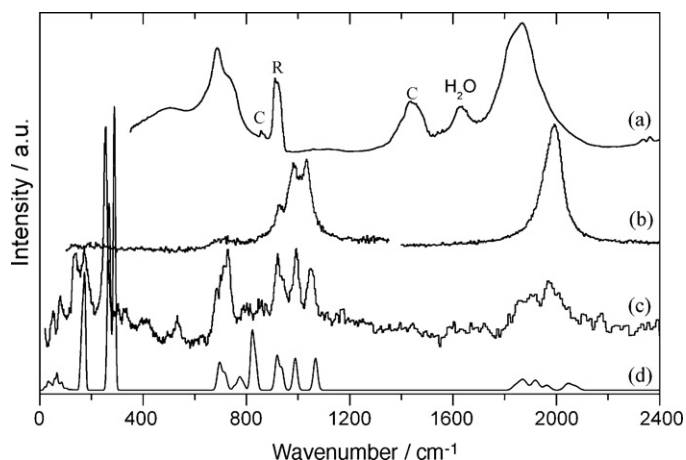
Fig. 9. (a) Infrared, (b) Raman, (c) INS spectra of Ba[ReH$_9$] and (d) INS spectrum generated from a calculation across the complete Brillouin zone. In (a) decomposition products are marked as C (carbonate) and R (rhenate). In (b) the range 100 – 1350 cm^{-1} is 2.5 times ordinate expanded relative to 1400 – 2400 cm^{-1}. Reproduced from Ref. [67] with permission of the American Chemical Society.

(IR: infrared active, R: Raman active, ia: inactive in both infrared and Raman). As may be seen from Fig. 9a and b [67], many fewer modes are observed in the infrared and Raman spectra than predicted. Surprisingly, the INS spectrum, Fig. 9c [64,67] does not show clear evidence for the missing modes, thus many of the modes must be accidentally degenerate.

The isolated [ReH$_9$]$^{2-}$ ion has been the subject of both empirical [65] and ab initio [72] investigations, none of which provided unambiguous assignments. Detailed investigations by periodic DFT [67] of both the full unit cell of Ba[ReH$_9$] and the isolated [ReH$_9$]$^{2-}$ ion at the same level of approximation were carried out. In the latter case, the physical model was an interacting periodic array of ions, with a homogeneous positive charge to ensure electroneutrality. This showed that the long range Coulombic interactions resulted in an up shift of 100–150 cm^{-1}. The long ranged nature of the Coulombic interactions means that nearest-neighbour interactions are insufficient and that infinite lattice sums are required to sum the contributions from distant periodic replicas. Fig. 9d shows the INS spectrum (fundamentals only) generated from a calculation across the complete Brillouin zone, including longitudinal optic–transverse optic (LOTO) splitting. It can be seen that the agreement is generally good and this is particularly the case for the internal modes of the [ReH$_9$]$^{2-}$ ion. We note that the shape of the band at 925 cm^{-1} is well-produced. The only mode that is miscalculated is that at 823 cm^{-1} (observed at 731 cm^{-1}) and the error is only 12%, all the other internal modes are calculated with an error of less than 5%, which is typical for DFT calculations. The librational modes about the a and b axes are calculated at 287 and 289 cm^{-1}, significantly higher than the observed value of 172 cm^{-1}. This situation where the internal modes are calculated to good accuracy but the external modes (librations and translations) are less well described, is commonly found [38,44] and is ascribed to anharmonicity, largely because there appears to be no other explanation. (The same ab initio codes are able to accurately predict external modes in molecular crystals.)

To investigate the bonding, Mulliken charges and Born effective charges (sometimes known as dynamical charges) were calculated. The results are shown in Table 5. It can be seen that the hydrogen atoms have a hydridic character (charge of −0.2) and that the cap and prism hydrogen atoms are essentially identical. The rhenium carries a small positive charge of +0.47 in contrast to its formal charge of +7. The 5d-orbital occupancy of 6 electrons, is higher than for the neutral atom configuration indicating that these are the orbitals mainly involved in the bonding. The barium ion is closest to its formal charge of +2, while the electrons are largely lost from the 6s orbital as expected (the 2.03 electron occupancy for the s orbitals in Table 5 is a sum over the 5s and 6s orbitals), it is surprising that there is some occupancy of the 5d-orbitals, indicating some degree of covalency between the barium and the hydrogen. The Born effective charges give a more complex picture. As is common, the magnitudes are larger than the Mulliken static charges, and for rhenium the sign is opposite. The large magnitudes will give rise to significant polarization during vibration, which accounts for the substantial long ranged interaction observed. A large anisotropy in the charge tensors is apparent for hydrogen, but the traces are close to the Mulliken values. The anisotropy is indicative of directional covalent bonding to the Re atom, and the negative overall dynamical charge confirms the hydridic nature of the protons. Calculation of the shared electron counts confirms the covalent nature of the Re–H bond but also shows a clear distinction between the cap and prism hydrides; there is a small interaction between the barium ion and the nearest prism hydrides. These are somewhat more electron rich than the cap hydrides, perhaps accounting for the interaction. The shared electron counts show that there is essentially zero interaction between the hydrides, confirming the assignment as a polyhydride, rather than as a mixed hydride dihydrogen complex. The work clearly demonstrates that to understand the spectroscopy and hence gain insight into the bonding, it is essential to use ab initio methods that explicitly include the intermolecular interactions; at present, periodic DFT is the best available method.

From Table 4, some of the same trends noted for the octahedral [TH$_6$]$^{n-}$ complexes are also observed. For all the [ReH$_9$]$^{2-}$ complexes, the frequencies occur in the same ranges for the internal modes, for the external modes there is more variation with counter-ion, although the limited data means that these conclusions should be treated with circumspection. For A$_2$[PdH$_2$] (A = Li, Na) and A$_2$[PtH$_4$] (A = Na, K, Rb) the frequencies decrease with the heavier counter-ion, presumably the same effect of the alkali metal ion accepting increased charge is operative as seen for the A$_2$[PtH$_6$] complexes [38]. On going from K$_2$[PdH$_4$] to K$_2$[PtH$_4$] the frequencies increase [34], as seen for Mg$_2$[TH$_6$] (T = Fe, Ru, Os). The opposite trend is seen for Mg$_2$[NiH$_4$] and Ba$_2$[PdH$_4$], the decrease caused by the heavier Ba ion outweighs that of going from Ni to Pd. This is supported by comparison with LaMg$_2$PdH$_7$ (which contains [PdH$_4$]$^{4-}$ ions [73]) where the decrease is much less than for the barium salt. (The stretching frequencies given for Ba$_2$[PdH$_4$] were obtained from periodic DFT calculations [35], these are somewhat higher, ∼10%, than the original assignments [56].)

The bonding in Mg$_2$[NiH$_4$] and Ba$_2$[PdH$_4$] has been investigated by periodic DFT [43]. The study showed that the bonding situation

Table 5
Atomic orbital populations, Mulliken charges and Born effective charges for Ba[ReH$_9$]. Reproduced from Ref. [67] with permission of the American Chemical Society.

Species	s	p	d	Total	Mulliken charge	Born effective charges
H$_{cap}$	1.20			1.20	−0.20	xx = −0.647 yy = 0.260 zz = 0.156
H$_{prism}$	1.21			1.21	−0.21	xx = −0.736 yy = 0.122 zz = 0.230
Re	0.33	0.19	6.01	6.53	+0.47	xx = −1.769 yy = −1.772 zz = −1.757
Ba	2.03[a]	6.00	0.60	8.63	+1.37	xx = 2.668 yy = 2.668 zz = 3.037

[a] Includes both 5s and 6s contributions.

in the two systems was quite different. For $Ba_2[PdH_4]$, the electronic density of states mirrors perfectly the molecular orbital states of the $[PdH_4]^{4-}$ ion, whereas for $Mg_2[NiH_4]$ a clear relation between the molecular orbital states of $[NiH_4]^{4-}$ ion and the density of states of the solid state compound is absent. The differences in bonding of $Mg_2[NiH_4]$ and $Ba_2[PdH_4]$ originate in the different strength of the M–H interactions (Pd–H interactions are considerably stronger than Ni–H ones) and in the different strength of the interaction between the alkaline earth metal component and hydrogen (Ba–H interactions are substantially weaker than those of Mg–H). $Mg_2[NiH_4]$ has a hydrogen capacity of 3.6 wt%, which is somewhat lower than the DOE target of 4.5 wt%, in addition the kinetics of adsorption and desorption are too slow to make the standard material viable. The introduction of defects should destabilise the Mg–H interactions and improve the kinetics. There has been a vast effort to introduce mechanical defects by ball milling, *e.g.* [76] and references therein, although chemical defects introduced by partial substitution of the magnesium should also be effective. The authors [43] suggested that while aluminium would be a good choice, they have successfully synthesised $Mg_2Na_2NiH_6$ [77] (better formulated as $\{Mg^{2+}\}_2\{Na^+\}_2\{H^-\}_2[NiH_4]^{4-}$) where the average length of the Ni–H bonds are considerably longer than in $Mg_2[NiH_4]$: 1.65 *vs.* 1.54 Å respectively. The complex has yet to be investigated by vibrational spectroscopy but would provide a fascinating comparison to $Mg_2[NiH_4]$.

Table 4 also shows what is so far a unique occurrence, complexes with the same formal oxidation state but different numbers of coordinated hydrides. The series $A_2[PdH_2]$ (A = Li, Na), $NaBa[PdH_3]$ and $Ba_2[PdH_4]$ contains Pd(0) with 2, 3 and 4 hydrides. The stretching frequencies decrease with increasing number of hydrides and based on force field models and *ab initio* calculations, the authors [43] concluded that this was the result of the Pd–H bond order decreasing in the order 1/2, 1/3, 1/4. The apparent force constant also showed a reasonable correlation with $1/(d_{Pd-H})$ where d_{Pd-H} is the Pd–H distance. The work emphasises that while hydride structures are often compared with halides, caution must be considered not too take this analogy too far. Hydrogen is unique with its low electron affinity from filling the K shell. This differentiates hydrides from other compounds, such as oxides or halides, where the energy gain from filling a conventional octet more strongly localizes the electrons. Although the radii of fluoride and hydride ions are similar, there are only two electrons in the latter. This results in the large polarizability and the unique softness of H^-, leading to what Pearson [78] expresses as a very low resistance to the deformation of the electron density. The stability, and for $NaBa[PdH_3]$ and $Ba_2[PdH_4]$ also their existence, could be ascribed to bonding between the hydrogen atoms of the complexes and the cations surrounding the complexes. In homoleptic hydrido complexes the large polarizability of hydrogen, *i.e.* the low resistance to a deformation of its electron density, can stabilise low valent metals by distributing electron density away from the central atom [43]. The work again highlights the crucial role of the counter-ion in ternary metal hydrides.

Palladium and platinum are also the only elements where it has been possible to make homoleptic hydrido complexes in more than one oxidation state. For Pd, using the same analysis as for the zero valent complexes [43], the Pd–H bond order in the Pd(II) $[PdH_4]^{2-}$ ion is calculated as ½ and the frequencies are close to those of $Li_2[PdH_2]$. For Pt the frequencies in Pt(II) $K_2[PtH_4]$ and Pt(IV) $K_2[PtH_6]$ are almost identical. Thus for a given metal it appears that the oxidation state does not greatly affect the frequencies and, by implication, the bonding is very similar.

Fig. 3 shows the structures of $Mg_2[FeH_6]$ (top), $Mg_2[CoH_5]$ (middle) and $Mg_2[NiH_4]$ (bottom). It can be seen that the structures are very similar, essentially as hydrides are removed the lattice distorts but maintains a roughly cubic form. This provides an opportunity to examine how the frequencies change while

the heavy atom structure is kept (approximately) the same. The similarity of the structure is indicated by the translational modes of the Mg^{2+} ion. These occur at 223 cm^{-1} in $Mg_2[FeH_6]$, 208 cm^{-1} in $Mg_2[CoH_5]$ and 234 and 193 cm^{-1} in $Mg_2[NiH_4]$.

The M–H bondlengths are similar (Fe–H = 1.556 Å [58], Co–H = 1.59 Å (apical), 1.515 Å (basal) [74], Ni–H = 1.572, 1.524, 1.538, 1.519 Å [75]) in all three complexes. The stretching and bending modes follow the pattern Fe > Co > Ni and track the formal oxidation state: Fe (II), Co(I) and Ni(0). The librational frequencies follow Co > Ni > Fe. This is more difficult to rationalise. The librational frequencies are inversely proportional to the moments of inertia, which are $I_a = I_b = I_c = 9.762$ amu Å^2 for $[FeH_6]^{4-}$, $I_a = I_b = 7.247$ amu Å^2, $I_c = 12.034$ amu Å^2 for $[CoH_5]^{4-}$ and $I_a = 5.87745$ amu Å^2, $I_b = 6.517$ amu Å^2, $I_c = 6.688$ amu Å^2 for $[NiH_4]^{4-}$. The stiffness of the potential in which the ion rotates will be determined by the Mg–H distances which are 2.278 Å for Fe and range from 2.170 to 2.402 Å for Co and 1.973 to 2.331 Å for Ni. Both effects would predict the order Ni > Co > Fe rather than that observed: Co > Ni > Fe.

Table 4 also includes complexes that contain interstitial hydrides, such as $LaMg_2PdH_7$ [73] and Rb_3TH_5 (T = Zn, Pt) [79,80]. These are more accurately described as $\{La^{3+}\}\{Mg^{2+}\}_2\{H^-\}_3\{[PdH_4]^{4-}\}$ and $\{Rb^+\}_3\{H^-\}\{[TH_4]^{2-}\}$ respectively. The translational modes of the interstitial hydrides are observable by vibrational spectroscopy but are difficult to assign. On the basis of force field calculations the interstitial hydride motions in Rb_3ZnH_5 were originally assigned to a weak feature at 561 cm^{-1} [70], subsequent periodic DFT calculations [71] have shown that the modes are in the range 690–720 cm^{-1} and mix with the bending modes of the $[PdH_4]^{4-}$ ion. This again emphasises that even sophisticated force field calculations that take into account librational and translational motions are inadequate to describe these systems; only periodic DFT calculations produce reliable results. Similarly, periodic DFT calculations of $LaMg_2PdH_7$ [35] have shown that the interstitial hydride motions occur in the range 700–1200 cm^{-1}. In this case the modes are strongly mixed with those of the $[PdH_4]^{4-}$ ion, at the lower energy with the bending modes and at the higher energy with the stretch modes.
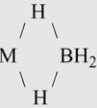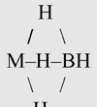
5. Borohydrides, alanates and gallates

The borohydrides (containing the tetrahedral $(BH_4)^-$ ion, confusingly also called tetrahydroborates or boranates) and alanates (containing the tetrahedral $(AlH_4)^-$ ion) are the most actively researched hydride compounds at present [81,82]. The reasons for this are apparent from Fig. 1: the compounds in the top right hand corner have the most desirable properties in terms of amount of hydrogen and hydrogen density and this is the territory of the borohydrides and alanates.

An isolated $(MH_4)^-$ ion has tetrahedral, T_d, symmetry. The nine vibrations are distributed as the non-degenerate ν_1 of a_1 symmetry which is the totally symmetric in-phase M–H stretch, doubly degenerate ν_2 of e symmetry which is the symmetric in-phase H–M–H bend, triply degenerate ν_3 of t_2 symmetry which is the antisymmetric M–H stretch and triply degenerate ν_4 of t_2 symmetry which is the antisymmetric H–M–H bend. The interpretation of the spectra is complicated by the fact that the bending modes occur at almost half the wavenumber of the stretching modes, consequently Fermi resonance between ν_1 and the a_1 component of $2\nu_2$ and also between ν_3 and the t_2 component of $2\nu_2$ occurs.

5.1. Alkali metal borohydrides

The borohydride ion forms a large number of compounds with many of the elements, including the alkali metals, alkaline earths,

Table 6
Fundamental vibrational transitions commonly observed for mononuclear $M(BH_4)_n$ configurations. Adapted from Ref. [83] with permission of the American Chemical Society.

Structure	Energy (cm^{-1})	Approx. type of internal coordinate	Infrared intensity	Raman intensity
Monodentate M–H–BH$_3$	2300–2450	B–H$_t$ stretching	Strong, probably a doublet	Strong
	~2000	B–H$_b$ stretching	Strong	Strong
	~2000–1700	M–H$_b$ stretching	May be very broad	May be broad
	1000–1150	BH$_3$ deformation	Strong band, possibly with weaker one at slightly higher wavenumber	Strong
Bidentate	2400–2600	B–H$_t$ stretching	Strong doublet, 50-80 cm^{-1} splitting	Strong singlet, possible shoulder
	1650–2150	B–H$_b$ stretching	Strong band, possible shoulder	Medium-strong band
	1300–1500	Bridge stretching	Strong, broad	Strong, broad
	1100–1200	BH$_2$ deformation	Strong,	Medium-strong, possibly a doublet
Tridentate	2450–2600	B–H$_t$ stretching	Strong singlet	Strong singlet
	2100–2200	B–H$_b$ stretching	Doublet, 50–80 cm^{-1} splitting	Strong singlet, possible shoulder
	1050–1150	Bridge deformation	Strong,	Strong singlet
Ionic M^{n+} $n(BH_4)^-$	2200–2300	B–H$_t$ stretching	Strong, broad	Strong, broad
	1050–1150	BH$_2$ deformation	Strong, broad	Weak

transition metals, lanthanides and actinides. The compounds can be ionic, as with the alkali metals and alkaline earths or borohydride can form monodentate (one M–H–B bridge), bidentate (two M–H–B bridges) or tridentate (three M–H–B bridges) compounds as well as polymeric materials with linking bidentate bridges. The monomeric compounds are readily distinguished by vibrational spectroscopy as shown in Table 6 [83]. It can be seen that the different modes of bonding give rise to different ranges vibrational energies that in concert with the intensity information allow distinction between the various forms.

As the focus of this review is on materials relevant to hydrogen storage media, the discussion will be restricted to the alkali metal, alkaline earth and aluminium borohydrides. The transition metal, lanthanide and actinide compounds have been comprehensively reviewed (including the vibrational spectra) [83,84]. The enormous chemistry [85] of the neutral borohydrides, B_xH_y ($x, y \geq 2$) and their anions is beyond the scope of this review.

As shown in Table 7, vibrational spectroscopy has been used extensively to investigate the borohydrides. Most investigations have used infrared and/or Raman spectroscopy and given the large absorption cross section of ^{10}B (3835 barn, 20% natural abundance, for comparison the absorption cross section of ^{11}B is 0.0055 barn) and ^{6}Li (940 barn, 7.5% natural abundance, the absorption cross section of ^{7}Li is 0.0454 barn), it might be expected that any neutron work whether diffraction or INS would require the use of the favourable isotope, *e.g.* as was done in [89] where ^{7}Li[^{11}BH$_4$] was used for both types of measurement. This is not the case and it is possible to obtain data [87,106] from natural abundance materials, albeit at some cost in signal-to-noise ratio.

Li(BH$_4$) has been extensively studied [86–90]. This exists in a low temperature orthorhombic phase (*Pnma*, $Z=4$) below 380 K and a hexagonal phase ($P6_3mc$, $Z=2$) from 384 K to the melting point at 541 K. Recent work has employed Raman spectroscopy and since the crystals are centrosymmetric in both phases, at most, only half of the modes are observed. Cooling to 5 K results in significant sharpening of the bands, which has allowed the detection of most of the Raman allowed modes and their assignment by periodic-DFT [90]. Low temperature (80 K) infrared spectra [86] are consistent with the Raman data and show that the factor group splitting is ~10 cm^{-1}. Translation modes are readily observed in both the infrared and Raman spectrum, the librations are more difficult to detect, although there are allowed modes. They can be observed by INS spectroscopy [87,89] and inferred from a Fermi resonance

enhanced second overtone at 1254 cm^{-1} in the infrared spectrum [88].

A very detailed Raman study [90] of the temperature dependence of the position, linewidth and intensity of the modes in the orthorhombic phase from 5 to 300 K has been performed. Analysis of several of the internal and external modes indicated strong anharmonic coupling between the modes. This is manifested in the non-linear thermal expansion of the orthorhombic phase [91]. The work particularly highlighted the anomalous behaviour of a mode at 148.8 cm^{-1} which was assigned to a B_{3g} libration. Periodic-DFT shows that the 148.8 cm^{-1} (calculated at 155.3 cm^{-1}) mode consists of synchronous in-phase rotation of $(BH_4)^-$ ions in the (b, c) plane and antiphase rotation between planes along a. This eventually leads to breaking of the *Pnma* symmetry and to the transition to the $P6_3mc$ phase [90,91].

Heating the orthorhombic phase into the hexagonal phase results in a simpler spectrum with much broader bands. Synchrotron diffraction studies [92] suggest that a nearly isotropic disorder of the rigid tetrahedral $(BH_4)^-$ ions is one of the factors stabilizing the hexagonal structure, such disorder would also account for the linewidth of the vibrational modes. Spectroscopic evidence for the onset of dynamic disorder of the $(BH_4)^-$ tetrahedron above the transition temperature was obtained from a study of the temperature dependence of the Raman linewidths during a heating and cooling cycle [88]. The linewidths of the modes increase abruptly at the phase transition during heating and decrease abruptly during cooling. Apart from some hysteresis, the spectra are completely reversible. Furthermore, the rate of increase of the bandwidths as a function of temperature is higher above than below the phase transition. This behaviour is a likely indication for coupling between the internal modes and the librations. A combined INS and periodic-DFT study [93] found that for energies <120 cm^{-1}, the phonon density of states of Li(^{11}BH$_4$) in the low temperature phase depends quadratically on the phonon energy while for the high temperature phase a linear dependence is observed, indicating anharmonicity in the high temperature phase. The increase in the phonon density of states at low energies in the high temperature phase as compared to the low temperature phase provides direct evidence for disorder in the hydrogen sub-lattice in the high temperature phase of Li(^{11}BH$_4$), which can originate from orientational disorder of $(BH_4)^-$ ions. The potential energy landscape for rotation of the $(BH_4)^-$ ions indicates that fairly localized minima and with barriers >4800 cm^{-1} exist in the low-temperature phase resulting in ordered $(BH_4)^-$ ions. In

Table 7
Observed frequencies and assignments for borohydrides with Groups I, II or III counter-ions.

| Hydride	Wt% H	Crystal structure (Z)[a] (Range/K)	Metal geometry[b] (symmetry)[b]	Stretching modes	Bending modes	Librational modes	Translational modes	Reference
Li(BH$_4$)	18.5	$P6_3mc$ ($Z=2$) (380–540)	Distorted tetrahedral (C_{3v})	(R): 2355, 2299, 2167	(R): 1302, 1096			[88]
		$Pnma$ ($Z=4$) (0–380)	Distorted tetrahedral (C_s)	(R): 2319, 2298, 2273 (IR): 2350, 2307, 2277	(R): 1320, 1290, 1240, 1098 (IR): 1089	(INS) 420 (IR) 418	(R): 282, 192, 150, 119, 96 (IR): 391, 324, 274, 232, 176, 162	[86–90]
Na(BH$_4$)	10.7	$Fm\bar{3}m$ ($Z=1$) (>190)	Tetrahedral (T_d)	(R): 2340, 2321 (IR): 2284	(R): 1274, 1124 (IR): 1110	(INS) 313 (R) 325 ± 15	(INS) 220, 140 (IR) 180	[87,104]
		$P42/nmc$ ($Z=2$) (<190)	Tetrahedral (D_{2d})	(R): 2341, 2322 (IR): 2302	(R): 1280 (IR): 1122	(INS) 240, 350 (IR) 384	(INS) 142, 88 (IR) 172	[103,106]
K(BH$_4$)	7.5	$Fm\bar{3}m$ ($Z=1$) (>65–70)	Tetrahedral (T_d)	(R): 2312, 2288 (IR): 2270	(R): 1246, 1119 (IR): 1112	(INS) 286 (R) 282 ± 15	(INS) 190, 75 (IR) 180	[87,104]
		$P42/nmc$ ($Z=2$) (<65–70)	Tetrahedral (D_{2d})	(R): 2314, 2291 (IR): 2281	(R): 1252, 1122 (IR): 1112	(INS) 320	(INS) 187, 82 (IR) 178	[103,106]
Rb(BH$_4$)	4.0	$Fm\bar{3}m$ ($Z=1$) (>22)	Tetrahedral (T_d)	(R): 2300, 2273 (IR): 2260	(R): 1234, 1112 (IR): 1106	(INS) 273 (R) 291 ± 15	(INS) 174 (IR) 170	[87,104]
Cs(BH$_4$)	2.7	$Fm\bar{3}m$ ($Z=1$) (>35)	Tetrahedral (T_d)	(R): 2287, 2255 (IR): 2244	(R): 1220, 1103 (IR): 1094	(INS) 272 (R) 291 ± 15	(INS) 115 (IR) 150	[87,104]
Be(BH$_4$)$_2$	20.3	$I4_1cd$ ($Z=8$)	Tetrahedral (C_1)	(R): 2509, 2450, 2330, 2125, 2093 (IR): 2510, 2451, 2330, 2113, 2075	(R): 1537, 1420, 1166, 1130, 1012, 722, 640, 582, 522 (IR): 1543, 1440, 1128, 1007, 970, 725, 640, 610, 555, 405		(R): 315, 266, 202 (IR) 319, 180	[113]
Mg(BH$_4$)$_2$	14.9	$P6_1$ ($Z=30$) (<453)	Tetrahedral (C_1)	(R): 2308, 2283 (IR): 2292, 2223	(R): 1310, 1288, 1205, 1190, 1126, 1088, 1039 (IR): 1400, 1262, 1126		(R): 670, 350, 248, 204, 195, 172 (IR):	[114,117]
	14.9	$Fddd$ ($Z=16$) (453 < 613 dec)	Tetrahedral (C_1)	(R): 2360, 2340, 2300 (IR): 2292, 2223	(R): (IR): 1400, 1262, 1126			[116,117]
Ca(BH$_4$)$_2$	11.6	$F2dd$ ($Z=2$) (<453 K)	Tetrahedral (C_2)	(R): 2414, 2352, 2327, 2272 (IR): 2451, 2315, 2253	(R): 1327, 1241, 1204, 1117, 1089 (IR): 1325, 1229, 1193 1110, 1075	(R): 475, 340, 298, 252, 218	(R): 111, 54	[122]
		$P4_2/m$ or $P\bar{4}$ ($Z=2$) (>453 K)	Tetrahedral (C_s or C_1)	(R): 2395, 2288 (IR): 2308, 2248, 2208	(R): 1310, 1254, 1081 (IR): 1323, 1282, 1231, 1193 1110, 1074			[122]
Al(BH$_4$)$_3$	16.9	$C2/c$ ($Z=8$) (0 < 180 K)	Tetrahedral (C_1)	(R): 2550, 2475, 2059 (IR): 2544, 2469, 2059, 2026	(R): 1511, 1422, 1155, 1146, 1113, 1105, 968 (IR): 1531, 1419, 1103, 966			[126]

[a] Number of formula units in the *primitive* unit cell.
[b] The metal geometry is the symmetry of the (BH$_4$)$^-$ ion, the point group in brackets is that of the crystallographic site symmetry.

contrast, the high temperature structure shows shallow barriers of $\sim$1600 cm^{-1} without distinct energy minima, so the orientation of a single $(BH_4)^-$ ion cannot be precisely defined.
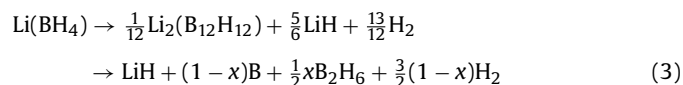
Vibrational spectroscopy has also been used to investigate the hydrogen desorption/adsorption processes. In its simplest form this is given by [94]:

$$Li(BH_4) \rightarrow LiH + (1-x)B + \tfrac{1}{2}xB_2H_6 + \tfrac{3}{2}(1-x)H_2 \qquad (2)$$
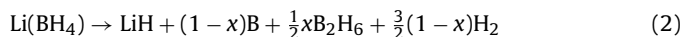
Infrared and Raman spectroscopies have two major advantages for this type of study: they are sensitive to both crystalline and amorphous materials, in contrast to diffraction methods, and they can follow a system across a change of state: solid to liquid processes (and *vice versa*) are readily studied. While nuclear magnetic resonance (NMR) is also sensitive to both amorphous and crystalline materials, it can only study one element at a time, vibrational spectroscopy is more democratic and sees everything. NMR can be used for either solids or liquids but cannot follow a process that involves a change of state (in a single experiment): this ability is restricted to optical techniques, particularly infrared and Raman spectroscopies.

In a highly imaginative use of Raman spectroscopy, Borgschulte et al. [94] followed the Raman spectra of $Li(BH_4)$ heated in D_2 and of $Li(BD_4)$ heated in H_2. The authors concluded that the diffusing species was a hydrogen (deuterium) atom and were able to determine the diffusion coefficient. They proposed that this was associated with defects which consist of BH_3 vacancies, *i.e.* $(BH_4)^-$ vacancies, which have been refilled with H^-. (Diborane desorption has been observed at temperatures below the melting point, explaining the formation of the vacancies.) The single hydrogen anion is assumed to be easily exchanged by deuterium, which then exchanges with one hydrogen of the neighbouring $(BH_4)^-$ anion. This mechanism agrees with the observed behaviour of the hydrogen–deuterium exchange, which is coupled to the desorption process. It can also explain the desorption reaction of B_2H_6 from solid $Li(BH_4)$.

In reality, the hydrogen desorption process is more complex than Eq. (2) suggests. The presence of an intermediate in the dehydrogenation process has been predicted theoretically [95] and observed experimentally by Raman spectroscopy [96]. The intermediate is most likely to be $Li_2(B_{12}H_{12})$, in the Raman spectrum bands are observed at 600–1000 cm^{-1} and 2500 cm^{-1}, these are lower and higher respectively than the corresponding B–H bending and stretching modes in $Li(BH_4)$ and are in reasonable agreement with those expected [95] and observed experimentally [97] for $Li_2(B_{12}H_{12})$. The presence of $Li_2(B_{12}H_{12})$ has been further confirmed by ^{11}B NMR [98] for a range of borohydride systems. Thus the desorption process is better represented as [95]:

$$Li(BH_4) \rightarrow \tfrac{1}{12}Li_2(B_{12}H_{12}) + \tfrac{5}{6}LiH + \tfrac{13}{12}H_2$$
$$\rightarrow LiH + (1-x)B + \tfrac{1}{2}xB_2H_6 + \tfrac{3}{2}(1-x)H_2 \qquad (3)$$

The vibrational spectra of the $(B_{12}H_{12})^{2-}$ ion in solution and in the solid state [99] for the potassium and caesium salts have been studied. The INS spectra of the lithium [97] and caesium salts [100] are distinctly different, reflecting the stronger interaction of the Li^+ ion with the anion.

The major difficulties with using $Li(BH_4)$ (and many other materials) for hydrogen storage are the poor reversibility and the thermodynamic and kinetic limitations which manifest as the need for high temperatures and the slow release and adsorption of H_2. To improve the properties, reducing the dimensions of the materials to the nanoscale is considered to be a promising approach. One way to achieve this, is to encapsulate the hydride in a porous material. This has the twin advantages of limiting the particle size and preventing particle agglomeration occurring during dehydrogenation/hydrogenation cycles at elevated temperatures, the
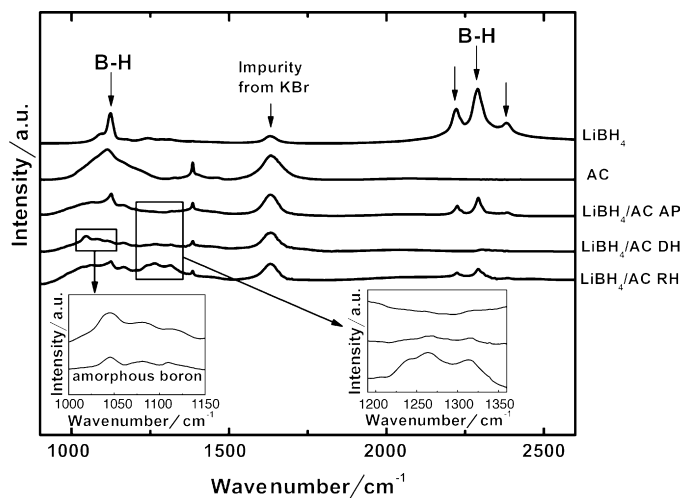

Fig. 10. Infrared spectra of the $Li(BH_4)$ encapsulated in amorphous carbon (AC) samples in the as-prepared (AP), after dehydrogenation at 623 K *in vacuo* (DH) and after re-hydrogenation at 573 K under 5 MPa of H_2 (RH) states, respectively. The spectra of pure $Li(BH_4)$ and amorphous carbon are also shown for comparison. Two insets are also included to show regions of interest more clearly. Reproduced from Ref. [101] with permission from Elsevier.

disadvantage is that the overall wt% hydrogen decreases because of the adsorbent.

Infrared spectroscopy [101] was used to follow the desorption/adsorption process for $Li(BH_4)$ encapsulated in amorphous carbon as shown in Fig. 10. The disappearance and re-emergence of the characteristic B–H modes of $Li(BH_4)$ clearly evidenced that the dehydrogenation reactions were reversible under the applied conditions. Several weak and broad modes were also detected in the 1000–1350 cm^{-1} region of the dehydrogenated and re-hydrogenated samples. By comparison to amorphous boron (left inset of Fig. 10), the weak bands in the 1000–1150 cm^{-1} range were assigned to amorphous boron in the dehydrogenated sample. Close examination of the infrared spectra found that new bands in the 1220–1350 cm^{-1} range appeared in the dehydrogenated sample and gained intensity after the re-hydrogenation reaction (right inset of Fig. 10). In a parallel study of a mechanically milled $Li(BH_4)$/graphite mixture, these bands were not observed in the sample after being dehydrogenated at 723 K. The results suggest that the unknown infrared bands originate from a Li–B–H intermediate species generated in the dehydrogenation/re-hydrogenation process, rather than from a reaction between the component elements of $Li(BH_4)$ and carbon. Interestingly, the new bands do not match those of $Li_2(B_{12}H_{12})$, suggesting that other intermediates may be present.

The remaining alkali metal borohydrides have been much less studied [102–107]. This is presumably a consequence of their lower wt% hydrogen content and higher hydrogen desorption temperatures. The room temperature structures of $M(BH_4)$ (M = Na, K, Rb, Cs) have cubic symmetry. Neutron diffraction [104,108] on the deuterides shows that the alkali cations and $(BD_4)^-$ anions form a NaCl type arrangement. Four deuterium atoms, on the average, surround boron at the corners of a boron-centered cube which is consistent with a random orientation of $(BD_4)^-$ about $\langle 1\,1\,1 \rangle$ directions. At 190 K and 65–70 K in the sodium and potassium salts respectively, the $(BD_4)^-$ ions order to give a tetragonal phase. There is evidence that the rubidium and caesium salts behave similarly at 22 and 35 K respectively, but the data were insufficient to allow unambiguous structure determination.

As shown in Fig. 11, Table 7 and implied by Table 6, the transition energies of the modes do not vary very much with the counter-ion, M^+. There is a small decrease with increasing size of M^+, which can
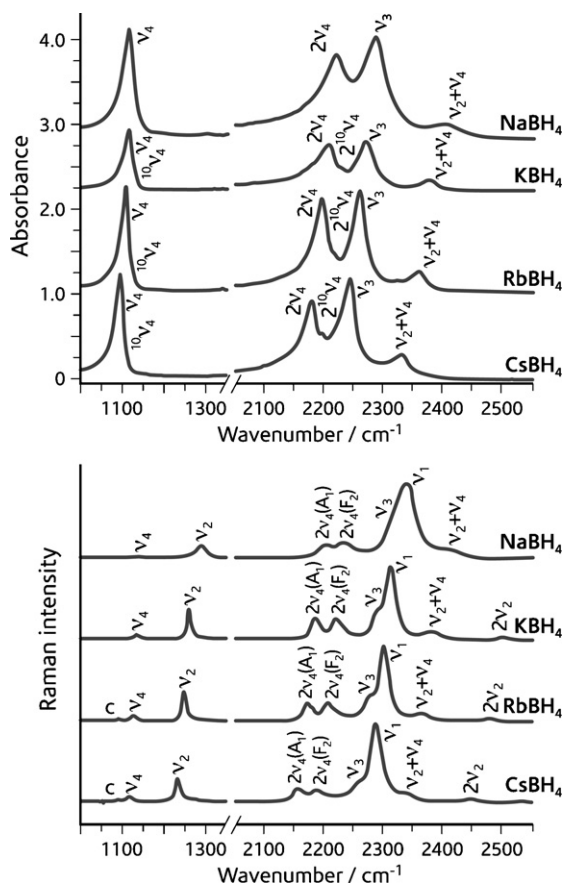
Fig. 11. Infrared (upper), and Raman (lower) spectra at room temperature for the alkali metal borohydrides M(BH$_4$) (M = Na, K, Rb, Cs). For clarity only some of the ^{10}B components are shown. Bands labelled C correspond to carbonate impurities present in the starting alkaline hydroxides. Reproduced from Ref. [104] with permission from Elsevier.

be ascribed to the lengthening of the B–H bond. The spectroscopic data are in agreement with the room temperature structural data as shown by the linear plot [104] of Badger's rule [109] which states that:

$$\nu_1^{-2/3} \propto d_{(B-D)} \tag{4}$$

where $d_{(B-D)}$ is the crystallographically determined B–D distance. Li$^+$ is anomalous but the crystal structure is different from that of its congeners. Fig. 11 also highlights the complications caused by the Fermi resonance between the overtones of the bending modes and the stretching modes in both the infrared and the Raman spectra.

Orimo et al. [82,96] noted that there is a correlation between the electronegativity of the cation and the frequency of the bending and stretching modes of hydrogen in the anion, although disentangling this from the anion size effect just noted is very difficult. They also noted a correlation with the hydrogen desorption (decomposition) temperature of the salt: Li (653 K) < Na (838 K) < K (857 K) < Rb, Cs (873 K).

All of the alkali metal borohydrides have been studied by Raman spectroscopy over the temperature range 300–540 K [105]. From the variation of the linewidth of ν_2 with temperature the authors were able to determine the barrier to reorientation and that it decreases with increasing cation size. The available space for the (disordered) tetrahedral (BH$_4$)$^-$ anions in the octahedral alkaline metal cavities increases when passing from the sodium to the cesium compound. The same conclusion was reached in an INS study [87], although the values were systematically higher (by a factor close to 1.8) than those derived from the Raman data. The INS

derived barriers were calculated from the observed libration energies and incorrect structural data and increases the barrier heights by ∼10%. The remaining discrepancy is not understood. The best fit to the data for the lithium salt requires two barriers and is again a consequence of the non-cubic nature of the structure.

5.2. Alkaline earth and aluminium borohydrides

Alkaline earth borohydrides are known for Be, Mg and Ca. Be(BH$_4$)$_2$ is unusual in that it can be volatilised. The structure of the gas phase species has been the subject of intense study by a variety of techniques including vibrational spectroscopy [110]. High level *ab initio* studies [111] suggest that there are two species present: a D_{3d} structure with a six coordinate Be from two tridentate borohydrides and a D_{2d} structure with a four coordinate Be from two bidentate borohydrides, with the D_{3d} structure marginally, ∼4 kJ mol^{-1}, more stable.

In the solid state Be(BH$_4$)$_2$ is polymeric [112] with chains of doubly bridging bidentate borohydrides and a third bidentate borohydride coordinated to the Be. Thus each Be is six coordinate. The vibrational spectra [113] show features that match the pattern expected for a bidentate borohydride (see Tables 6 and 7), although the spectra are more complex because of the bridging borohydrides. The 20.3 wt% hydrogen of Be(BH$_4$)$_2$ would be of enormous interest, were it not for the acute toxicity of beryllium and its compounds.

Mg(BH$_4$)$_2$ is of considerable current interest because of its 14.9 wt% hydrogen. The structure was only solved recently [114,115] and is unusually complex: there are 30 formula units (330 atoms) in the hexagonal ($P6_1$) ambient temperature phase, above 453 K, it transforms to an orthorhombic (*Fddd*) phase with 16 formula units (176 atoms) in the primitive unit cell. In both phases, the magnesium has an unusual eightfold coordination. The vibrational spectra show that it is clearly an ionic borohydride, as can be seen from Tables 6 and 7. The infrared spectra are remarkably similar in both phases [116], consistent with the almost identical local arrangement of corner-sharing tetrahedra with magnesium ions at the centre and (BH$_4$)$^-$ anions at the vertices [115]. *Ab initio* calculations [156] suggest that the low temperature structure is actually $P6_122$, a supergroup of $P6_1$. These are very difficult to distinguish from powder diffraction data, unfortunately the complexity of the unit cells means that vibrational spectroscopy is not helpful either. The Raman spectra have also been investigated as a function of pressure [117] and evidence for phase transitions was observed.

Ca(BH$_4$)$_2$ is also of interest because although the wt% hydrogen is lower (11.5), it can be synthesised by the reaction:

$$CaH_2 + MgB_2 + 5H_2 \leftrightarrows Ca(BH_4)_2 + MgH_2 \tag{5}$$
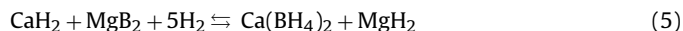
which can absorb or release 8.3 wt% hydrogen [118]. Ca(BH$_4$)$_2$ can be obtained by other routes and exhibits a variety of structures. The most stable is the orthorhombic α-phase with the boron atoms on C_2 sites, the most recent synchrotron data [119] indicates that the space group is *F2dd*, rather than the *Fddd* originally reported [120], this transforms to the β-phase above 453 K which is described as either $P\bar{4}$ [119] or $P4_2/m$ [121]. A γ-phase is also known and depending on the conditions a mixture of phases can be obtained.

The vibrational spectra have been comprehensively investigated [122] and as can be seen from Table 7, the spectra conform to that expected for an ionic borohydride. In particular, the intensity pattern in the infrared and Raman spectra of the deformation modes is similar to that observed for Li(BH$_4$) [86–90]. Upon heating α-Ca(BH$_4$)$_2$, between 294 and 450 K the bands at 218 and 298 cm^{-1} shift to lower wavenumber by ∼10 cm^{-1} and broaden significantly while the position of the internal modes do not appear to be affected. These temperature dependent shifts (observed between 80 and 450 K) indicate significant anharmonic behaviour in the α-

Table 8
Bonding in selected borohydrides. Adapted from Ref. [115] with permission of the International Union of Crystallography.

	Ionic radius[a] (Å)	Number of coordinating (BH_4) groups	M–B (Å)	Number of coordinating H atoms	Type of bonding
Be	0.45	3	1.92–2.00	6	Covalent
Al	0.54	3	2.10–2.14	6	Covalent
Mg[b]	0.89	4	2.34–2.49	8	Ionic
Li	0.92	4	2.47–2.54	9	Ionic
Ca[c]	1.34	6	2.91–2.98	12	Ionic
Na[d]	1.39	6	3.07	12	Ionic
K	1.64	6	3.35	12	Ionic

[a] Ionic radii from Shannon [129].
[b] Values are the same for both the high and low temperature phases.
[c] Values are the same for both the α and β-phases.
[d] Room temperature structure.

phase. Close to the α → β transition, the spectra show a continuous transition to the high temperature phase.

The Raman line width in the bending mode region at room temperature of the two bands at 1327 and 1241 cm^{-1} is 11 and 8 cm^{-1} respectively for the α-form. In contrast, the half-width at half-maximum of the two bands at 1310 and 1254 cm^{-1} of the β-form is 26.5 and 21 cm^{-1} respectively. By analogy with the behaviour observed for the alkali borohydrides [93,105], this suggests the presence of some disorder caused by reorientational motions of the $(BH_4)^-$ ion in the β-phase, in agreement with recent crystallographic work [121].

The infrared spectrum [122] of a mixture of β- and γ-Ca$(BD_4)_2$ shows several partly resolved bands at 2250, 2330 and 2380 cm^{-1} which can be assigned to individual $(H–BD_3)^-$ stretching modes arising from hydrogen impurities in the deuterated sample. In principle, each of these bands corresponds to a different B–H bond length, thus in this sample, there are at least three different B–H bond lengths, one being somewhat longer (hence a weaker force constant) than the others. This well illustrates the sensitivity of vibrational spectroscopy to very small changes in bond distances: the crystallography shows all the B–H bond distances to lie in the range 1.16–1.18 Å [119].

Al$(BH_4)_3$ resembles Be$(BH_4)_2$ in that it is readily volatised to give a gas phase structure with bidentate (BH_4) groups [123]; it differs from Be$(BH_4)_2$ in that this structure is retained in both the liquid and solid states [124–126]. In the solid state, Al$(BH_4)_3$ undergoes a phase transition at ~180 K, although the geometry of the Al$(BH_4)_3$ molecule itself varies little between the two phases, the principal difference relates to the packing of the molecular units [124]. The molecule occupies a C_1 site but approximates to D_{3h} symmetry. In the gas phase it is suggested that the symmetry is D_3 with the D_{3h} form being the transition state [124].

The vibrational spectroscopy has been extensively investigated, the most comprehensive work studied all three phases and used multiple isotopic substitution [125,126]. The gas phase infrared spectroscopy is surprising: the spectra show only broad vibrational bands, with no trace of resolved rotational structure [127]. The extreme spectral congestion observed is believed to arise primarily from splittings of the ground state and the upper vibrational levels of modes that couple to the torsional motions and to other low energy modes of the (BH_4) groups.

The gas phase, liquid, solid state and matrix isolated spectra [125,126] are remarkably similar and show only minor wavenumber shifts between the phases. The spectra have been assigned by *ab initio* calculations of the isolated molecule [128] assuming D_3 symmetry. Although there are eight molecules in the primitive unit cell, the factor group splitting is small and the assignments are probably valid for the solid state as well.

From Table 8 [115], it can be seen that as the ionic radius and the ionic character of the metal increase, the number of coordinating (BH_4) groups increases from three to four to six. There is also a clear

distinction between ionic and covalent borohydrides in terms of the M–B distance.

5.3. Alanates

Interest in the alanates as hydrogen storage materials was sparked by the report [130] that titanium compounds catalysed both the adsorption and desorption of H_2 in Na(AlH_4). This initiated renewed activity in the study of these compounds and in particular, the role of the Ti-dopant.

The structures and hydrogen adsorption/desorption behaviour of the alanates have been recently reviewed [81,82,131]. Alkali metal alanate salts, M(AlH_4), are known for all the alkali metals. The Li salt is monoclinic ($P2_1/c$) with the Al on a C_1 site [132], the Na salt is tetragonal ($I4_1/a$) with the Al on a S_4 site [133], the K salt is orthorhombic ($Pnma$) with the Al on a C_s site [134], the Rb and Cs salts are also orthorhombic [131] with presumably the same structure as the K salt. In all cases where the hydrogen coordination has been determined, even though the Al site symmetry is not T_d the coordination is only slightly distorted from tetrahedral.

Table 9 gives the observed frequencies and assignments for the alkali metal alanates [135–145]. The general trend is that the Al–H stretching frequencies decrease with increasing mass of the counter-ion. The changes in structure as the counter-ion is varied Li → Na → K/Rb/Cs mean that the frequencies do not follow a monotonic trend, in particular, the totally symmetric stretching mode for K(AlH_4) (1779 cm^{-1}) is at higher energy than that of Na(AlH_4) (1762 cm^{-1}) [145]. The bending frequencies are largely unchanged by the counter-ion, the degree of splitting of the mode depends on both the structure and the counter-ion.

The transition energies observed in the Raman spectrum for the stretching modes of Na(AlH_4) show a degree of variability. They are given as: 1770 and 1680 cm^{-1} [140], 1769 and 1680 cm^{-1} [141], 1773 and 1684 cm^{-1} [143], 1762 and 1681 cm^{-1} [144] and 1762 and 1683 cm^{-1} [145]. In addition weak shoulders at 1815 cm^{-1} [140] and 1782 cm^{-1} [140] have been reported and assigned to stretching modes. The latter two assignments are not supported by periodic-DFT calculations [139,143] which indicate that the highest energy mode is ~1770 cm^{-1}. A more plausible assignment is to the first overtone of the bending mode ν_4 (which will include a totally symmetric component) that is observed because its intensity is enhanced by Fermi resonance with the totally symmetric stretch.

The spectroscopy gives a conflicting result to the crystallography: one of the Al–H bonds is shorter in the potassium salt than in either the lithium or sodium salt, yet the wavenumber is lower than that of the lithium salt. Interestingly, periodic-DFT calculations [139] of K(AlH_4) do not reproduce the dissimilar bondlengths found in the neutron diffraction study [134].

The INS spectra [139] for Li(AlH_4) and Na(AlH_4) for the 0–1200 cm^{-1} region are shown in Fig. 12. The spectra are clearly complex and show evidence for dispersion in the modes indicat-

Table 9
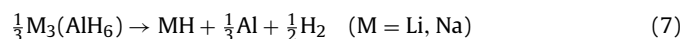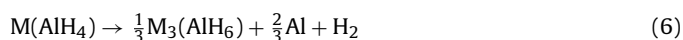Observed frequencies and assignments for alanates with Group I or II counter-ions.

Hydride	Wt% H	Crystal structure (Z)[a] (Range (K))	Metal geometry (symmetry)[b]	Stretching modes	Bending modes	Librational modes	Translational modes	Reference
Li(AlH$_4$)	10.6	$P2_1/c$ (Z = 4) (0 < 423 K)	Tetrahedral (C$_1$)	(R): 1837, 1762, 1722 (IR): 1800, 1780, 1645	(R): 950, 882, 830, 780, 690 (IR): 890, 810, 700	(R): 510, 438, 322 (IR): 465 (INS): 504, 476, 437, 357, 312	(R): 220, 165, 151, 143, 112, 95 (INS): 230, 204, 162, 145, 123, 106, 89	[135–139]
Na(AlH$_4$)	7.5	$I4_1/a$ (Z = 2) (0 < 425 K)	Tetrahedral (S$_4$)	(R): 1762, 1681 (IR): 1680	(R): 848, 817, 770 (IR): 900, 800, 735, 690	(R): 521, 429 (INS): 544, 506, 474, 445, 400	(R): 180, 125, 117 (INS): 189, 148, 138, 107	[135,136,140–145]
K(AlH$_4$)	5.8	$Pnma$ (Z = 4)	Tetrahedral (C$_s$)	(R): 1779, 1711 (IR): 1715	(R): 790 (IR): 811, 729			[135,145]
Rb(AlH$_4$)	3.5	$Pnma$ (Z = 4)[c]	Tetrahedral (C$_s$)[c]	(IR): 1715	(IR): 811, 769, 729			[135]
Cs(AlH$_4$)	2.5	$Pnma$ (Z = 4)[c]	Tetrahedral (C$_s$)[c]	(IR): 1711	(IR): 741			[135]
Li$_3$(AlH$_6$)	11.2	$R\bar{3}$ (Z = 2)	Octahedral (C$_{3i}$)	(R): 1604, 1311 (IR): 1410, 1300	(R): 1014, 975 (IR): 1000, 960, 854	(R): 577, 510		[146]
Na$_3$(AlH$_6$)	5.9	$P2_1/n$ (Z = 2)	Octahedral (C$_i$)	(R): 1556, 1465 (IR): 1440, 1290	(R): 990, 815, 760 (IR): 930, 842, 690	(R): 560, 480		[146]
K$_2$Li(AlH$_6$)	5.1	$R\bar{3}m$ (Z = 2)	Octahedral (D$_{3d}$)	(R): 1519	(R): 1174, 1097, 948	(R): 502, 394	(R): 270, 145, 135	[147]
Mg(AlH$_4$)$_2$	9.3	$P\bar{3}m1$ (Z = 4) (0 < 135 K)	Tetrahedral (D$_3$)	(R): 1969, 1944, 1808 (IR): 1835	(R): 824, 768, 736			[153,154]
Ca(AlH$_4$)$_2$	7.9	$Pbca$ (Z = 8)[d]	Tetrahedral (C$_1$)	(IR): 1788	(IR): 816, 653	(IR): 482		[159]

[a] Number of formula units in the *primitive* unit cell.
[b] The metal geometry is the symmetry of the (MH$_x$)$^{n-}$ ion, the point group in brackets is that of the crystallographic site symmetry.
[c] Assuming that the structure is the same as that of the potassium salt.
[d] Structure based on comparison of the X-ray powder pattern with an *ab initio* prediction [158,159].
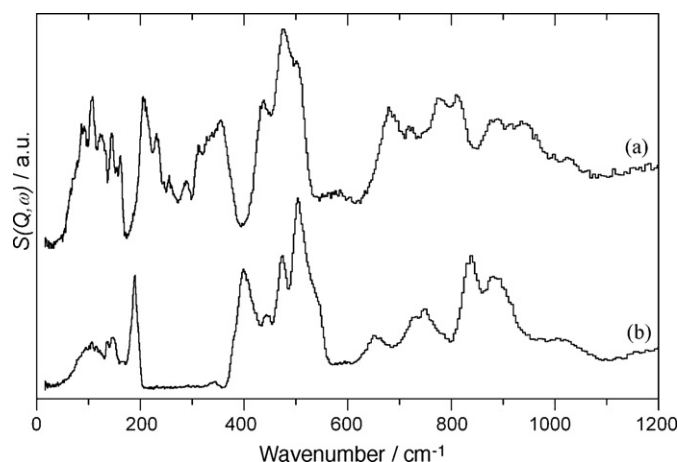
Fig. 12. INS spectra of (a) Li(AlH$_4$) and (b) Na(AlH$_4$).

ing significant long range interactions in the crystal [139,142]. A periodic-DFT study of Li(AlH$_4$) [139] shows that there is 0.08 shared electrons between the Li$^+$ and one of the hydrides. The lithium salt's spectrum is unusual in that there is no clear break between the translations and the librations, as is clearly seen between 200 and 350 cm^{-1} in the sodium salt. This is a consequence of the light mass of lithium; the lithium translational modes occur in the range 200–400 cm^{-1} and mix with the alanate librational modes at ~500 cm^{-1}. Although lithium has no significant scattering cross section, the coupling between the lithium translational modes and the librational modes of the alanates results in strong features in the INS spectrum for the lithium modes. This is demonstrated by generating the vibrational transition energies of a (hypothetical) isotope of lithium with a mass of 100. The lithium translational modes suffer a large drop in energy, which dramatically reduces the coupling with the alanate librational modes, consequently a gap opens up between the translational and librational modes as the coupling is reduced [139].

The chemistry of the alanates differs from that of the borohydrides in that both lithium and sodium form complexes of the type M$_3$(AlH$_6$) with octahedral (AlH$_6$)$^{3-}$ ions [144–146]. The alkali metal ions occupy different crystallographic sites and fully ordered mixed salts M$_2$M'(AlH$_6$) with M = Na, K and M' = Li, Na are known [147].

M$_3$(AlH$_6$) are stable, isolable compounds but also occur as intermediates in the decomposition of the M(AlH$_4$) (M = Li, Na) salt:

$$M(AlH_4) \rightarrow \tfrac{1}{3}M_3(AlH_6) + \tfrac{2}{3}Al + H_2 \qquad (6)$$

$$\tfrac{1}{3}M_3(AlH_6) \rightarrow MH + \tfrac{1}{3}Al + \tfrac{1}{2}H_2 \quad (M = Li, Na) \qquad (7)$$

These release 5.3 and 2.6 wt% H$_2$ for M = Li and 3.8 and 1.9 wt% H$_2$ for M = Na, for reactions (6) and (7) respectively, relative to the parent M(AlH$_4$)]. As with palladium, Table 4, increasing the coordination number in the same oxidation state results in a decrease in the M–H stretching wavenumber. This is a consequence of the longer Al–H bondlength in the hexahydrides. There is a linear correlation between the highest energy of the normal mode and the shortest Al–H bond distance in the hydrides [145].

The mechanism of the transformation of the tetrahydride into the hexahydride has been investigated [145,148,149]. Li$_3$(AlH$_6$) can be formed by reaction of M(AlH$_4$) with LiH. Reaction with LiD produces partly deuterated materials Li$_3$(AlH$_x$D$_{6-x}$). Bureau et al. [148,149] found that neither Li$_3$(AlH$_3$D$_3$) nor Li$_3$(*cis*-AlH$_4$D$_2$) (or Li$_3$[*cis*-AlH$_2$D$_4$] if Li(AlD$_4$) and LiH were used) were formed, only the *trans* isomer was obtained. They concluded that the (AlH$_4$)$^-$ ion flattens under the influence of two D$^-$ ions that interact simultaneously with the aluminium to generate the hexahydride [149]. For the sodium salt it was observed that new peaks appeared in the
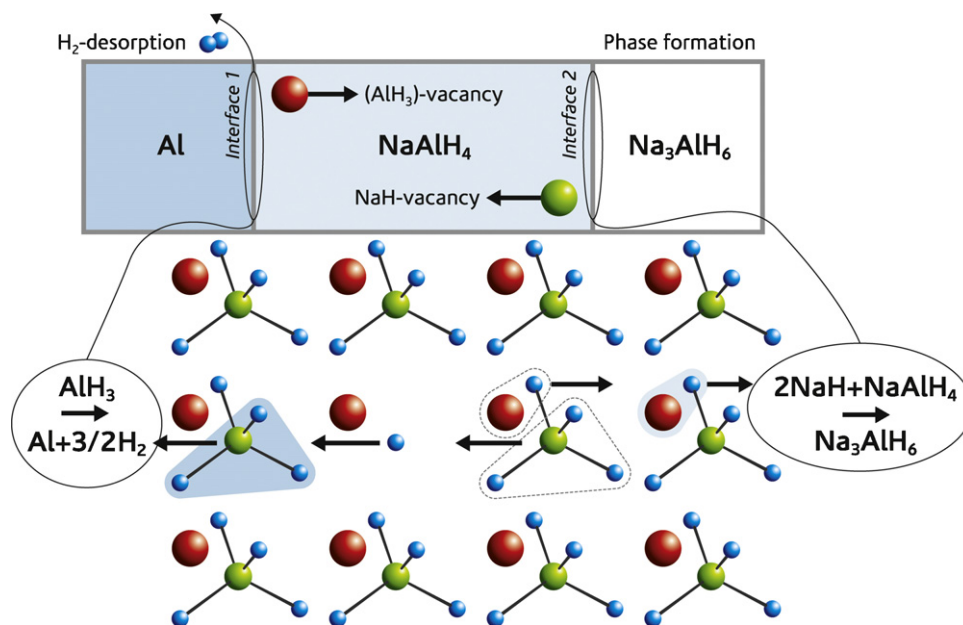
Fig. 13. Sketch of the decomposition reaction of Na(AlH$_4$) via vacancy diffusion in Na(AlH$_4$). Possible vacancies are, *e.g.* charge-neutral species such as AlH$_3$ and NaH. At the interface, a vacancy is formed, this is filled by the corresponding atoms from the inner phase, producing the same vacancy one layer deeper in the bulk, in this way the vacancy moves through the crystal. Reproduced from Ref. [150] with permission of the PCCP Owner Societies.

Raman spectrum at 1562, 1114 and 987 cm^{-1} [145]. It was suggested that reaction occurs in the melt and that the Na$^+$ interacts with one of the H$^-$ in (AlH$_4$)$^-$ and a local structure of (NaH–AlH$_3$) is formed in the liquid Na(AlH$_4$). The resulting distorted AlH$_3$ species may be one possibility to explain the new bands in the Raman spectrum upon melting.

Investigation of the effect of doping with titanium (and other metal) salts has extensively used vibrational spectroscopy. One of the advantages of vibrational spectroscopy is that it is not restricted to crystalline systems, thus small amounts of amorphous material are readily detectable. The Raman and infrared spectra [144] and the INS spectrum [142] of titanium doped Na(AlH$_4$) are very similar to those of the pure compound, suggesting that the effect is not a weakening of the Al–H bond by substitution of Ti^{3+} for Na$^+$. A combination of thermogravimetry, mass spectrometry and Raman spectroscopy [150] were used to gain understanding of the surface processes, diffusing species and the formation of intermediates by studying the exchange of hydrogen for deuterium. The authors conclude that the results are consistent with a vacancy mediated process. The role of the titanium is to dissociate H$_2$ which then reacts with metallic aluminium to form volatile AlH$_x$ species. Evidence for these was seen in an INS study of the rehydriding of hydrogen-depleted Na(AlH$_4$) [151]. Fig. 13 shows a sketch of the proposed model.

Alanates of magnesium, calcium and strontium are also known [Ref. [81] and refs. therein]. In the structure of the magnesium salt, three of the Al–H bonds are longer (1.634 Å) than the fourth (1.606 Å) [152]. The three long bonds bridge the Al and Mg ions, forming a sheet and the fourth points into the interlayer space. This has the result that the short Al–H bond has a much higher vibrational wavenumber [153,154] than is usually seen for the alanates (Table 9) in essence it becomes an uncoupled oscillator. The behaviour is similar to that of the bridging borohydrides, Table 6. The strength of the Mg–H–Al bond is less than that of the Mg–H–B bond because the spectra are markedly less perturbed than in Mg(BH$_4$)$_2$. The vibrational spectra of Mg(AlH$_4$)$_2$ have been comprehensively assigned by periodic-DFT [155].

Her et al suggested [115] that the more covalent nature of the (BH$_4$)$^-$ unit versus (AlH$_4$)$^-$ may contribute to the complexity of the Mg(BH$_4$)$_2$ structure compared with that of the compositionally similar Mg(AlH$_4$)$_2$. Bader charge analysis was used by Dai et al. [156] to obtain the average charge distribution of atoms in Mg(AlH$_4$)$_2$ and the low temperature Mg(BH$_4$)$_2$ phase. According to the calculations, each aluminium atom gives up ~2.15 electrons compared with 1.53 electrons for the boron atoms. Likewise, the charge on the hydrogen atoms in the Mg(AlH$_4$)$_2$ structure is −0.74, compared with −0.59 for hydrogen atoms in Mg(BH$_4$)$_2$. Hence, B–H bonds are more covalent than Al–H bonds. However, as noted by Dai et al. [156] this does not explain how more covalent bonding leads to more complex structures.

Mg(AlH$_4$)$_2$ may be prepared by ball milling AlH$_3$ and MgH$_2$ or by metathesis of Na(AlH$_4$) and MgCl$_2$ in diethyl ether or THF. The latter method results in solvates that can be dried to give the unsolvated material. The solvate molecules interact with the (AlH$_4$)$^-$ as shown by the change in the Al–H stretching wavenumber [153]:

$$1731\,\text{cm}^{-1}(\text{diethyl ether}) < 1795\,\text{cm}^{-1}(\text{THF})$$

$$< 1835\,\text{cm}^{-1}(\text{unsolvated}).$$

This is similar to what is seen with Mg$_2$[FeH$_6$] and its soluble derivatives [46,60–62] (Table 1).

Calcium and strontium alanates have been much less investigated. The structure of Ca(AlH$_4$)$_2$ was predicted by periodic–DFT [157] and a comparison of the X-ray powder pattern is consistent with the prediction [158]. The only vibrational spectroscopic data is the infrared spectrum of Ca(AlH$_4$)$_2$ [159] which is very similar to that of Mg(AlH$_4$)$_2$.

Calcium and strontium alanates decompose to an intermediate MAlH$_5$ phase which contains chains of vertex sharing (AlH$_6$) octahedra [158]. These compounds and their formation from the alanates have not yet been investigated by vibrational spectroscopy but it is clearly a process that is ripe for such a study.

5.4. Gallates

The gallates containing the (GaH$_4$)$^-$ ion are not of interest for hydrogen storage applications but are included here for comparison with (BH$_4$)$^-$ and (AlH$_4$)$^-$. Table 10 lists the limited data that is

Table 10
Observed frequencies and assignments for gallates with Group I counter-ions.

Hydride	Wt% H	Crystal structure (Z)[a]	Metal geometry[b] (symmetry)[b]	Stretching modes	Bending modes	Reference
Na(GaH$_4$)	4.2	$Cmcm$ (Z = 2)	Tetrahedral (C_{2v})	(R): 1830, 1750 (IR): 1775, 1750	(R): 865, 760 (IR): 720, 575	[136,160]
K(GaH$_4$)	3.6	$Pnma$ (Z = 4)	Tetrahedral (C_s)	(R): 1800, 1771, 1719 (IR): 1717	(R): 834, 760 (IR): 760, 710	[136,160]
Rb(GaH$_4$)	2.6		Tetrahedral	(R): 1799, 1760, 1725 (IR): 1733	(R): 835, 763 (IR): 765, 710	[160]
Cs(GaH$_4$)	2.0		Tetrahedral	(R): 1785, 1750, 1725 (IR): 1723	(R): 821 (IR): 760, 720	[160]

[a] Number of formula units in the *primitive* unit cell.

[b] The metal geometry is the symmetry of the (GaH$_4$)$^-$ ion, the point group in brackets is that of the crystallographic site symmetry.

available. The structures of the sodium [161] and potassium [162] salts (the rubidium and caesium salts are believed to have the same structure as the potassium salt [160]) show isolated (GaH$_4$)$^-$ tetrahedra and the spectra are completely consistent with these. As seen in other systems, there is a dependency on the nature of the counter-ion although this is not especially strong for the gallates. This is presumably a consequence of all the salts being largely ionic so there is little specific (as opposed to Coulombic) interaction in the lattice.

For the sequence Na(MH$_4$) the highest wavenumber is at 2340 cm^{-1} (M = B), 1782 cm^{-1} (M = Al) and 1830 cm^{-1} (M = Ga), the potassium salts also follow the same pattern. While there is no explanation of this unusual pattern, it was noted [160] that the electronegativities of the atoms follow the same order.

6. Conclusions

As this review demonstrates, there has been, and there is still ongoing, a considerable amount of work on the vibrational spectroscopy and the properties of the ternary metal hydrides. Much of the work has been carried out in the last decade, prompted by the intensive search for suitable hydrogen storage materials. In a ternary metal hydride, while the central atom is the most important determinant of the properties, it has become increasingly clear that the counter-ion is much more than just a spectator, it often plays a key role in determining the stability of the material. As such, varying the counter-ion provides an important mechanism for optimising the desired properties.

The current trend in hydrogen storage research is to more complex systems [3]. Amides and imides of Li, Mg and Al and their mixtures are being actively studied [163]. Mixtures of binary hydrides and borohydrides (known as reactive hydride composites, RHC) are also of interest, the most studied of which is MgH$_2$ + Li(BH$_4$) [164,165]. A more complex mixture that includes LiNH$_2$ offers improved kinetics at a lower desorption temperature [166]. A variety of other materials are also under active investigation including perovskites such as NaMgH$_3$ [167], ammonia borane H$_3$NBH$_3$ [168] and its alkali metal derivatives [169].

In addition, to materials discovery there is also an intense effort in materials optimisation involving catalysed desorption and adsorption and mechano-chemical treatment of materials. In all these areas vibrational spectroscopy has played an important part and will continue to do so. Its advantages lie in its flexibility; it is not restricted to crystalline systems, amorphous or nanocrystalline materials are readily observable, it is amenable to *in situ* studies, it is democratic; infrared and Raman spectroscopy are not element specific and uniquely among probes they are able to follow a reaction across a change of state.

Vibrational spectroscopy and *ab initio* calculations are a synergistic pairing. Comparison of computed and experimental spectra provides a stringent test of the calculation, while the calculation provides unambiguous assignments of the spectra. INS spectra provide the most reliable test since they only require the amplitude of motion of the atoms in each mode. The accuracy of computed infrared spectra are rapidly improving and while Raman spectra are not yet routinely available for periodic systems, this is only a question of time.

References

[1] D.S. Scott, Int. J. Hydrogen Energy 29 (2004) 225.
[2] http://www1.eere.energy.gov/hydrogenandfuelcells/storage/pdfs/targets_onboard_hydro_storage.pdf.
[3] A. Züttel, A. Borgshulte, L. Schlapbach (Eds.), Hydrogen as a Future Energy Carrier, Wiley-VCH, Weinheim, 2008.
[4] E.M. Gray, Advan. Appl. Ceramics 106 (2007) 25.
[5] H.G. Schimmel, G. Nijkamp, G.J. Kearley, A. Rivera, K.P. de Jong, F.M. Mulder, Mater. Sci. Eng. B: Solid State Mater. Adv. Technol. 108 (2004) 124.
[6] V.V. Struzhkin, B. Militzer, W.L. Mao, H. Mao, R.J. Hemley, Chem. Rev. 107 (2007) 4133.
[7] N.L. Rosi, J. Eckert, M. Eddaoudi, D.T. Vodak, J. Kim, M. O'Keeffe, O.M. Yaghi, Science 300 (2003) 1127.
[8] X. Lin, J. Jia, X. Zhao, K.M. Thomas, A.J. Blake, G.S. Walker, N.R. Champness, P. Hubberstey, M. Schröder, Angew. Chem. Int. Ed. 45 (2006) 735.
[9] Y. Fukai, The Metal–Hydrogen System, Basic Bulk Properties, Springer Series in Materials Science, vol. 21, Springer-Verlag, Heidelberg, 2005.
[10] E. Wicke, H. Brodowsky, H. Züchner, in: G. Alefield, J. Vlkl (Eds.), Hydrogen in Intermetallic Compounds II. Surface and Dynamic Properties Applications, Topics in Applied Physics, vol. 67, Springer, Heidelberg, 1992.
[11] E.M. Gray, T.P. Blach, C.E. Buckley, J. Alloys Compd. 293 (1999) 57.
[12] W. Bronger, G. Auffermann, Chem. Mater. 10 (1998) 2723.
[13] K. Yvon, G. Renaudin, in: R.B. King (Ed.), Encyclopedia of Inorganic Chemistry, second ed., John Wiley, New York, 2005, p. 1814.
[14] K. Yvon, Z. Kristallogr. 218 (2003) 108.
[15] G. Auffermann, P. Muller, W. Bronger, Z. Anorg. Allg. Chem. 630 (2004) 2113.
[16] A. Züttel, Mater. Today 6 (2003) 24.
[17] F.A. Cotton, G. Wilkinson, C.A. Murillo, M.M. Bochmann, Advanced Inorganic Chemistry, 6th ed., John Wiley, New York, 1999, p. 995 (Chapter 18-D-10).
[18] H.C. Brown, P.V. Ramachandran, Reductions in organic synthesis—recent advances and practical applications, ACS Symposium Series 641 (1996) 1.
[19] R.O. Moyer Jr., C. Staniski, J. Tanaka, M.I. Kay, R. Kleinberg, J. Solid State Chem. 3 (1971) 541.
[20] J.S. Thompson, R. Lindsay, R.O. Moyer Jr., Inorg. Chem. 14 (1975) 1866.
[21] M. Kritikos, D. Noréus, J. Solid State Chem. 93 (1991) 256.
[22] D. Noréus, K.W. Tornroos, A. Borje, T. Szabo, W. Bronger, H. Spittank, G. Auffermann, P. Muller, J. Less-Common Met. 139 (1988) 233.
[23] K. Kadir, D. Noréus, Z. Phys. Chem. N.F 163 (1989) 231.
[24] M. Olofsson, M. Kritikos, D. Noréus, Inorg. Chem. 37 (1998) 2900.
[25] M. Olofsson-Mårtensson, M. Kritikos, D. Noréus, J. Am. Chem. Soc. 121 (1999) 10908.
[26] K. Kadir, M. Kritikos, D. Noréus, A.F. Andersen, J. Less-Common Met. 172 (1991) 36.
[27] W. Bronger, G. Auffermann, J. Alloys Compd. 187 (1992) 87.
[28] E. Ronnebro, D. Kyoi, H. Blomqvist, D. Noréus, T. Sakai, J. Alloys Compd. 368 (2004) 279.
[29] D. Noréus, P.E. Werner, Acta Chem. Scand. A36 (1982) 847.
[30] V. Paul-Boncour, M. Latroche, A. Percheron-Guégan, J. Solid State Chem. 150 (2000) 183.
[31] V. Paul-Boncour, S.M. Filipek, M. Dorogova, F. Bourée, G. André, I. Marchuk, A. Percheron-Guégan, R.S. Liu, J. Solid State Chem. 178 (2005) 356.
[32] D. Bublitz, G. Peters, W. Preetz, G. Auffermann, W. Bronger, Z. Anorg. Allg. Chem. 623 (1997) 184.

[33] M.M. Barsan, I.S. Butler, D.F.R. Gilson, R.O. Moyer Jr., W. Zhou, H. Wu, T.J. Udovic, J. Phys. Chem. A 112 (2008) 6936.
[34] E. Suchanek, N. Lange, G. Auffermann, W. Bronger, H.D. Lutz, J. Raman Spectrosc. 30 (1999) 981.
[35] S.F. Parker, J.W. Taylor, H. Herman, J.-P. Rapin, N. Penin, K. Yvon, J. Alloys Compd. 470 (2009) 80.
[36] P.C.H. Mitchell, S.F. Parker, A.J. Ramirez-Cuesta, J. Tomkinson, Vibrational Spectroscopy with Neutrons, with Applications in Chemistry, Biology, Materials Science and Catalysis, World Scientific, Singapore, 2005.
[37] V.F. Sears, Neutron News 3 (1992) 26.
[38] S.F. Parker, S.M. Bennington, A.J. Ramirez-Cuesta, G. Auffermann, W. Bronger, H. Herman, K.P.J. Williams, T. Smith, J. Am. Chem. Soc. 125 (2003) 11656.
[39] E. Gerdau, H. de Waard (Eds.), Nuclear Resonant Scattering of Synchrotron Radiation, Hyperfine Interactions, vol. 123–124, Kluwer Academic, New York, 1999.
[40] M. Liao, Q. Zhang, Inorg. Chem. 36 (1997) 396.
[41] T.K. Firman, C.R. Landis, J. Am. Chem. Soc. 120 (1998) 12650.
[42] R.B. King, Coord. Chem. Rev. 200–202 (2000) 813.
[43] U. Häussermann, H. Blomqvist, D. Noréus, Inorg. Chem. 41 (2002) 3684.
[44] L.M.L. Daku, H. Hagemann, Phys. Rev. B 76 (2007) 014118.
[45] E. Orgaz, A. Aburto, J. Phys. Chem. C 112 (2008) 15586.
[46] S.F. Parker, K.P.J. Williams, M. Bortz, K. Yvon, Inorg. Chem. 36 (1997) 5218.
[47] H. Hagemann, R.O. Moyer Jr., J. Alloys Compd. 330–332 (2002) 296.
[48] R.O. Moyer Jr., R. Lindsay, D.N. Marks, in: R. Bau (Ed.), Transition Metal Hydrides, Advanced Chemistry Series, vol. 167, American Chemical Society, Washington, DC, 1978, p. 366.
[49] M.M. Barsan, R.O. Moyer Jr., I.S. Butler, D.F.R. Gilson, J. Alloys Compd. 424 (2006) 73.
[50] K. Nakamoto, Infrared and Raman Spectra of Inorganic and Coordination Compounds Part A: Theory and Applications in Inorganic Chemistry, fifth ed., Wiley-Interscience, New York, 1997, p. 214 (Chapter II-8).
[51] D.M. Yost, S.C.S. Steffens, S.T. Gross, J. Chem. Phys. 2 (1934) 311.
[52] S.F. Parker, J.B. Forsyth, J. Chem. Soc. Faraday Trans. 94 (1998) 1111.
[53] R.O. Moyer Jr., J.R. Wilkins, P. Ryan, J. Alloys Compd. 290 (1999) 103.
[54] G. Herzberg, Infrared and Raman Spectra, Van Nostrand Reinhold, New York, 1945, p. 214.
[55] R. Bau, M.H. Drabnis, Inorg. Chim. Acta 259 (1997) 27.
[56] M. Olofsson-Mårtensson, U. Häussermann, J. Tomkinson, D. Noréus, J. Am. Chem. Soc. 122 (2000) 6960.
[57] R.O. Moyer Jr., S.M. Antao, B.H. Toby, F.G. Morin, D.F.R. Gilson, J. Alloys Compd. 460 (2008) 138.
[58] J.-J. Didisheim, P. Zolliker, K. Yvon, P. Fischer, J. Scheffer, M. Gubelmann, A.F. Williams, Inorg. Chem. 23 (1984) 1953.
[59] R. Bau, M.Y. Chiang, D. Ho, S.G. Gibbins, T. Emge, T.F. Koetzle, Inorg. Chem. 23 (1984) 2823.
[60] D.E. Linn, G.M. Skidd, E.M. Tipman, Inorg. Chim. Acta 291 (1999) 142.
[61] D.E. Linn, G.M. Skidd, S.N. McVay, Inorg. Chem. 41 (2002) 5320 (see also supporting material for this paper).
[62] U. Bergmann, W. Sturhahn, D.E. Linn, F.E. Jenney, M.W.W. Adams, K. Rupnik, B.J. Hales, E.E. Alp, A. Mayse, S.P. Cramer, J. Am. Chem. Soc. 125 (2003) 4016.
[63] A.P. Ginsberg, C.R. Sprinkle, Inorg. Chem. 8 (1969) 2212.
[64] J.W. White, C.J. Wright, J. Chem. Soc. Faraday Trans. 68 (1972) 1414.
[65] J.A. Creighton, T.J. Sinclair, J. Chem. Soc. Faraday Trans. II 70 (1974) 548.
[66] N.T. Stetson, K. Yvon, J. Alloys Compd. 223 (1995) L4.
[67] S.F. Parker, K. Refson, K.P.J. Williams, D.A. Braden, B.S. Hudson, K. Yvon, Inorg. Chem. 45 (2006) 10951.
[68] S.F. Parker, J.C. Sprunt, U.A. Jayasooriya, M. Bortz, K. Yvon, J. Chem. Soc. Faraday Trans. 94 (1998) 2595.
[69] D. Noréus, J. Tomkinson, Chem. Phys. Lett. 154 (1989) 439.
[70] S.F. Parker, K.P.J. Williams, T. Smith, M. Bortz, B. Bertheville, K. Yvon, Phys. Chem. Chem. Phys. 4 (2002) 1732.
[71] S.F. Parker, K. Yvon, K. Refson, in: R. Withnall, B.Z. Chowdhry (Eds.), Proceedings of ICORS XXI, IM Publications, Chichester, 2008, p. 693.
[72] M. Shen, H.F. Schaefer III, H. Partridge, Mol. Phys. 76 (1992) 995.
[73] K. Yvon, J.-Ph. Rapin, N. Penin, Z. Ma, M.Y. Chou, J. Alloys Compd. 446–447 (2007) 34.
[74] P. Zolliker, K. Yvon, P. Fischer, J. Schefer, Inorg. Chem. 24 (1985) 4177.
[75] P. Zolliker, K. Yvon, J.D. Jorgensen, F.J. Rotella, Inorg. Chem. 25 (1986) 3590.
[76] R. Vijaya, R. Sundaresana, M.P. Maiyab, S.S. Murthy, Int. J. Hydrogen Energy 30 (2005) 501.
[77] K. Kadir, D. Noréus, Inorg. Chem. 46 (2007) 2220.
[78] R.G. Pearson, J. Chem. Educ. 64 (1987) 561.
[79] M. Bortz, A. Hewat, K. Yvon, J. Alloys Compd. 253–254 (1997) 13.
[80] W. Bronger, G. Auffermann, Z. Anorg. Allg. Chem. 621 (1995) 1318.
[81] F. Schüth, B. Bogdanovič, M. Felderhoff, Chem. Commun. (2004) 2249.
[82] S. Orimo, Y. Nakamori, J.R. Eliseo, A. Züttel, C.M. Jensen, Chem. Rev. 107 (2007) 4111.
[83] T.J. Marks, J.R. Kolb, Chem. Rev. 77 (1977) 263.
[84] T. Sato, K. Miwa, Y. Nakamori, K. Ohoyama, H.-W. Li, T. Noritake, M. Aoki, S. Towata, S. Orimo, Phys. Rev. B 77 (2008) 104114.
[85] N.N. Greenwood, A. Earnshaw, Chemistry of the Elements, Pergamon Press, Oxford, 1984, Ch. 6.4.
[86] K.B. Harvey, N.R. McQuaker, Can. J. Chem. 49 (1971) 3282.
[87] J. Tomkinson, T.C. Waddington, J. Chem. Soc. Faraday Trans. 272 (1976) 528.
[88] S. Gomes, H. Hagemann, K. Yvon, J. Alloys Compd. 346 (2002) 206.

[89] M.R. Hartman, J.J. Rush, T.J. Udovic, R.C. Bowman Jr., S.-J. Hwang, J. Solid State Chem. 180 (2007) 1298.
[90] A.-M. Racu, J. Schoenes, Z. Łodziana, A. Borgschulte, A. Züttel, J. Phys. Chem. A 112 (2008) 9716.
[91] J.Ph. Soulié, G. Renaudin, R. Černý, K. Yvon, J. Alloys Compd. 346 (2002) 200.
[92] Y. Filinchuk, D. Chernyshov, R. Černý, J. Phys. Chem. C 112 (2008) 10579.
[93] F. Buchter, Z. Łodziana, Ph. Mauron, A. Remhof, O. Friedrichs, A. Borgschulte, A. Züttel, D. Sheptyakov, Th. Strässle, A.J. Ramirez-Cuesta, Phys. Rev. B 78 (2008) 094302.
[94] A. Borgschulte, A. Züttel, P. Hug, A.-M. Racu, J. Schoenes, J. Phys. Chem. A 112 (2008) 4749.
[95] N. Ohba, K. Miwa, M. Aoki, T. Noritake, Y. Nakamori, S. Orimo, A. Züttel, Phys. Rev. B 74 (2006) 075110.
[96] S. Orimo, Y. Nakamori, N. Ohba, K. Miwa, M. Aoki, S. Towata, A. Züttel, Appl. Phys. Lett. 89 (2006) 021920.
[97] J.-H. Her, M. Yousufuddin, W. Zhou, S.S. Jalisatgi, J.G. Kulleck, J.A. Zan, S.-J. Hwang, R.C. Bowman Jr., T.J. Udovic, Inorg. Chem. 47 (2008) 9757.
[98] S.-J. Hwang, R.C. Bowman Jr., J.W. Reiter, J. Rijssenbeek, G.L. Soloveichik, J.-C. Zhao, H. Kabbour, C.C. Ahn, J. Phys. Chem. C 112 (2008) 3164.
[99] L.A. Leites, S.S. Bukalov, A.P. Kurbakova, M.M. Kaganski, Yu.L. Gaft, N.T. Kuznetsov, I.A. Zakharova, Spectrochim. Acta Part A: Mol. Spectrosc. 38 (1982) 1047.
[100] D.G. Allis, B.S. Hudson, J. Phys. Chem. A 110 (2006) 3744.
[101] Z.Z. Fang, P. Wang, T.E. Rufford, X.D. Kang, G.Q. Lu, H.M. Cheng, Acta Mater. 56 (2008) 6257.
[102] C.J.H. Schutte, Spectrochim. Acta 16 (1960) 1054.
[103] K.B. Harvey, N.R. McQuaker, Can. J. Chem. 49 (1971) 3272.
[104] G. Renaudin, S. Gomes, H. Hagemann, L. Keller, K. Yvon, J. Alloys Compd. 375 (2004) 98.
[105] H. Hagemann, S. Gomes, G. Renaudin, K. Yvon, J. Alloys Compd. 363 (2004) 126.
[106] D.G. Allis, B.S. Hudson, Chem. Phys. Lett. 385 (2004) 166.
[107] S. Orimo, Y. Nakamori, A. Züttel, Mater. Sci. Eng. B 108 (2004) 51.
[108] P. Fischer, A. Züttel, Mater. Sci. Forum 443–444 (2004) 287.
[109] R.M. Badger, J. Chem. Phys. 3 (1935) 710.
[110] J.W. Nibler, J. Am. Chem. Soc. 94 (1972) 3349.
[111] A. Derecskei-Kovacs, D.S. Marynick, Chem. Phys. Lett. 228 (1994) 252–258 (and references therein).
[112] D.S. Marynick, W.N. Lipscomb, Inorg. Chem. 11 (1972) 820.
[113] J.W. Nibler, D.F. Shriver, T.H. Cook, J. Chem. Phys. 54 (1971) 5257.
[114] R. Černý, Y. Filinchuk, K. Yvon, Angew. Chem. Int. Ed. 46 (2007) 5765 (see also supplementary material).
[115] J.-H. Her, P.W. Stephens, Y. Gao, G.L. Soloveichik, J. Rijssenbeek, M. Andrus, J.-C. Zhao, Acta Cryst. B63 (2007) 561.
[116] K. Chłopek, C. Frommen, A. Léon, O. Zabara, M. Fichtner, J. Mater. Chem. 17 (2007) 3496.
[117] L. George, V. Drozd, S.K. Saxena, E.G. Bardaji, M. Fichtner, J. Phys. Chem. C 113 (2009) 486.
[118] G. Barkhordarian, T.R. Jensen, S. Doppiu, U. Bösenberg, A. Borgschulte, R. Gremaud, Y. Cerenius, M. Dornheim, T. Klassen, R. Bormann, J. Phys. Chem. C 112 (2008) 2743.
[119] Y. Filinchuk, E. Rönnebro, D. Chandra, Acta Mater. 57 (2009) 732.
[120] K. Miwa, M. Aoki, T. Noritake, N. Ohba, Y. Nakamori, S. Towata, A. Züttel, S. Orimo, Phys. Rev. B 74 (2006) 155122.
[121] F. Buchter, Z. Łodziana, A. Remhof, O. Friedrichs, A. Borgschulte, Ph. Mauron, A. Züttel, D. Sheptyakov, G. Barkhordarian, R. Bormann, K. Chłopek, M. Fichtner, M. Sørby, M. Riktor, B. Hauback, S. Orimo, J. Phys. Chem. B 112 (2008) 8042.
[122] M. Fichtner, K. Chłopek, M. Longhini, H. Hagemann, J. Phys. Chem. C 112 (2008) 11575 (see also supporting material for this paper).
[123] A. Almenningen, G. Gundersen, A. Haaland, Acta Chem. Scand. 22 (1968) 328.
[124] S. Aldridge, A.J. Blake, A.J. Downs, R.O. Gould, S. Parsons, C.R. Pulham, J. Chem. Soc. Dalton Trans. (1997) 1007.
[125] A.R. Emery, R.C. Taylor, Spectrochim. Acta 16 (1960) 1455.
[126] D.A. Coe, J.W. Nibler, Spectrochim. Acta 29A (1973) 1789.
[127] A. Al-Kahtani, D.L. Williams, J.W. Nibler, S.W. Sharpe, J. Phys. Chem. A 102 (1998) 537.
[128] J.O. Jensen, Spectrochim. Acta 59A (2003) 1565.
[129] R.D. Shannon, Acta Cryst. A 32 (1976) 751.
[130] B. Bogdanović, M. Schwickardi, J. Alloys Compd. 253–254 (1997) 1.
[131] V.P. Tarasov, G.A. Kirakosyan, Russ. J. Inorg. Chem. 53 (2008) 2048.
[132] B.C. Hauback, H.W. Brinks, H. Fjellvåg, J. Alloys Compd. 346 (2002) 184.
[133] B.C. Hauback, H.W. Brinks, C.M. Jensen, K. Murphy, A.J. Maeland, J. Alloys Compd. 358 (2003) 142.
[134] B.C. Hauback, H.W. Brinks, R.H. Heyn, R. Blom, H. Fjellvåg, J. Alloys Compd. 394 (2005) 35.
[135] T.G. Adiks, V.V. Gavrilenko, L.I. Zakharkin, L.A. Ignat'eva, J. Appl. Spectrosc. 6 (1967) 546.
[136] A.E. Shirk, D.F. Shriver, J. Am. Chem. Soc. 95 (1973) 5904.
[137] J.-C. Bureau, J. Bonnetot, P. Claudy, H. Eddaoudi, Mater. Res. Bull. 20 (1985) 1147.
[138] J.-P. Bastide, J.-C. Bureau, J.-M. Létoffé, P. Claudy, Mater. Res. Bull. 22 (1987) 185.
[139] S.F. Parker, K. Refson, unpublished work.
[140] J.-C. Bureau, J.-P. Bastide, B. Bonnetot, H. Edaoudi, Mater. Res. Bull. 20 (1985) 93.

[141] D.J. Ross, M.D. Halls, A.G. Nazri, R.F. Aroca, Chem. Phys. Lett. 388 (2004) 430.
[142] J. Íñiguez, T. Yildirim, T.J. Udovic, M. Sulic, C.M. Jensen, Phys. Rev. B 70 (2004) 060101 (R).
[143] E.H. Majzoub, K.F. McCarty, V. Ozoliņš, Phys. Rev. B 71 (2005) 024118.
[144] S. Gomes, G. Renaudin, H. Hagemann, K. Yvon, M.P. Sulic, C.M. Jensen, J. Alloys Compd. 390 (2005) 305.
[145] H. Yukawa, N. Morisaku, Y. Li, K. Komiya, R. Rong, Y. Shinzato, R. Sekine, M. Morinaga, J. Alloys Compd. 446 (2007) 242.
[146] J.-C. Bureau, Z. Amri, P. Claudy, J.-M. Létoffé, Mater Res. Bull. 24 (1989) 23.
[147] E. Rönnebro, E.H. Majzoub, J. Phys. Chem. B 110 (2006) 25686.
[148] J.-C. Bureau, Z. Amri, P. Claudy, J.-M. Létoffé, Mater. Res. Bull. 24 (1989) 267.
[149] J.-C. Bureau, J.P. Bastide, P. Claudy, J.-M. Létoffé, Z. Amri, J. Less Common Met. 130 (1987) 371.
[150] A. Borgschulte, A. Züttel, P. Hug, G. Barkhordarian, N. Eigen, M. Dornheim, R. Bormann, A.J. Ramirez-Cuesta, Phys. Chem. Chem. Phys. 10 (2008) 4045.
[151] Q.J. Fu, A.J. Ramirez-Cuesta, S.C. Tsang, J. Phys. Chem. B 110 (2006) 711.
[152] A. Fossdal, H.W. Brinks, M. Fichtner, B.C. Hauback, J. Alloys Compd. 387 (2005) 47.
[153] M. Fichtner, J. Engel, O. Fuhr, A. Glöss, O. Rubner, R. Ahlrichs, Inorg. Chem. 42 (2003) 7060.
[154] M. Fichtner, J. Engel, O. Fuhr, O. Kircher, O. Rubner, Mater. Sci. Eng. B 108 (2004) 42.
[155] E. Spanò, M. Bernasconi, Phys. Rev. B 71 (2005) 174301.
[156] B. Dai, D.S. Sholl, J.K. Johnson, J. Phys. Chem. C 112 (2008) 4391.
[157] O.M. Løvvik, Phys. Rev. B 71 (2005) 144111.
[158] C. Weidenthaler, T.J. Frankcombe, M. Felderhoff, Inorg. Chem. 45 (2005) 3849 (see also supplementary material).
[159] H. Kabbour, C.C. Ahn, S.-J. Hwang, R.C. Bowman Jr., J. Graetz, J. Alloys Compd. 446–447 (2007) 264.
[160] A.P. Kurbakova, L.A. Leites, V.V. Gavrilenko, Yu.N. Karaksin, L.I. Zakharkin, Spectrochim, Acta Part A: Mol. Spectrosc. 31 (1975) 281.
[161] Yu.Z. Nozik, E.S. Kuklina, N.A. Bliznyuk, S.V. Borisov, Sov. Phys. Cryst. 36 (1991) 31.
[162] S.I. Bakum, A.V. Irodova, S.F. Kuznetsova, O.I. Lyakhovitskaya, Yu.Z. Nozik, V.A. Somenkov, Koord. Khim. 16 (1990) 1210.
[163] P. Chen, Z. Xiong, G. Wu, Y. Liu, J. Hu, W. Luo, Scripta Mater. 56 (2007) 817.
[164] J.J. Vajo, S.L. Skeith, J. Phys. Chem. B 109 (2005) 3719.
[165] M. Dornheim, S. Doppiu, G. Barkhordarian, U. Boesenberg, T. Klassen, O. Gutfleisch, R. Bormann, Scripta Mater. 56 (2007) 841.
[166] J. Yang, A. Sudik, D.J. Siegel, D. Halliday, A. Drews, R.O. Carter, C. Wolverton, G.J. Lewis, A. Sachtler, J.J. Low, S.A. Faheem, D.A. Lesch, V. Ozolins Angew, Chem. Intl. Ed. 47 (2008) 882.
[167] H. Wu, W. Zhou, T.J. Udovic, J.J. Rush, T. Yildirim, Chem. Mater. 20 (2008) 2335.
[168] A.C. Stowe, W.J. Shaw, J.C. Linehan, B. Schmid, T. Autrey, Phys. Chem. Chem. Phys. 9 (2007) 1831.
[169] Z. Xiong, C.K. Yong, G. Wu, P. Chen, W. Shaw, A. Karkamkar, T. Autrey, M.O. Jones, S.R. Johnson, P.P. Edwards, W.I.F. David, Nat. Mater. 7 (2007) 138.